Journal of Antivirals & Antiretrovirals
ISSN: 1948-5964
OPEN ACCESS Freely available online
Research Article

The HTLV-1 Latency-Maintenance Factor p30II Induces the Phosphorylation and Hypoxia-Independent Mitochondrial Targeting of TIGAR Analogous to Tyrosine Kinase Receptor-Signaling and Suppresses Oncogene-Induced Oxidative Toxicity

Robert Harrod[1*], Tetiana Bowley[1], Aditi Malu[1], Natalie M. Adams[1], Julia Savage[1], Melika Saberi[1], Mya VanderHagen[1], Reena Alame[1], Makenna Keating[1], Courtney Yates[2]

[1]Department of Biological Sciences, Southern Methodist University, Dallas, USA; [2]Department of Biological Sciences, Laboratory Animal Resource Center, Southern Methodist University, Dallas, USA

ABSTRACT

The Human T-Cell Leukemia Virus Type-1 (HTLV-1) is a complex oncoretrovirus that infects $CD4^+$ T-cells and causes an aggressive lympho-neoplastic disease, known as Adult T-Cell Leukemia/Lymphoma (ATLL). Our earlier studies have demonstrated that the HTLV-1 latency-maintenance factor p30II interacts with TIP60, prevents TIP60-mediated K120-acetylation of the TP53 protein, and induces hypoxia-independent mitochondrial targeting of the TP53-Induced Glycolysis and Apoptosis Regulator (TIGAR) a 2,6-bisfructose-phosphatase that suppresses the accumulation of damaging Reactive Oxygen Species (ROS) in proliferating cells. Here, we demonstrate that p30II induces serine-phosphorylation of the TIGAR associated with its targeting to mitochondrial membranes in HTLV-1-transformed ATLL lymphocytes. Our studies have further revealed that tyrosine kinase growth factor receptor-signaling similarly induces serine-phosphorylation and mitochondrial targeting of the TIGAR correlated with Myc-dependent cellular proliferation. These findings allude to a conserved mechanism for the modulation of TP53-dependent pro-survival functions by viral oncoproteins and mitogenic signals to protect proliferating cells against metabolic oxidative toxicity. Moreover, we demonstrate that lentiviral-siRNA-knockdown of TIGAR expression in immunodeficient NOD/scid mice engrafted with HTLV-1+ SLB1-Green Fluorescent Protein (GFP) tumor cells effectively inhibited lymphomagenesis and CNS metastasis *in vivo*, suggesting that TIGAR could be a plausible target for antiviral therapy to treat HTLV-1-associated cancers.

Keywords: HTLV-1; p30; Viral oncoprotein; ATLL; TIGAR; *p53*; c-Myc; Mitochondria; ROS; Phosphorylation

INTRODUCTION

The Human T-Cell Leukemia Virus Type-1 (HTLV-1) is a delta oncoretrovirus that infects and transforms $CD4^+$ T-cells and causes Adult T-Cell Leukemia/Lymphoma (ATLL) a rare, yet aggressive hematological malignancy often associated with therapy-resistance and almost invariably poor clinical outcomes. HTLV-1-infections are also etiologically linked to a progressive demyelinating neuroinflammatory disease, known as HTLV-1-Associated Myelopathy/Tropical Spastic Paraparesis (HAM/TSP), as well as several other auto-inflammatory diseases, including infectious dermatitis, rheumatoid arthritis, uveitis, keratoconjunctivitis, sicca syndrome, and Sjögren's syndrome. It is estimated there are 10-20 million HTLV-1-infected individuals worldwide with most living in the tropical equatorial regions of Southeast Asia (i.e., Japan, China, Taiwan, Malaysia, and the Philippines), Australia and Melanesia, Northern and Central Africa, the Middle East, Central and South America, and islands of the French West Indies in the Caribbean. In the United States, Hawaii and Florida have highest incidences of ATLL, due largely to early population migrations from HTLV-1 endemic areas [1-3].

The transmission of HTLV-1 typically requires direct intercellular contact with infected lymphocytes, as extracellular particles are poorly infectious, and occurs across a virological synapse, *via* intercellular conduits/nanotubules or viral surface biofilms [4-6]. Primary infection is most often postnatally from mother-to-infant through breastfeeding, but, similar to the Human Immunodeficiency Virus (HIV), HTLV-1 transmission can occur through sexual intercourse, intravenous

Correspondence to: Robert Harrod, Department of Biological Sciences, Southern Methodist University, Dallas, USA, E-mail: rharrod@smu.edu

Received: 22-Mar-2024, Manuscript No. JAA-24-30353; **Editor assigned:** 25-Mar-2024, PreQC No. JAA-24-30353 (PQ); **Reviewed:** 15-Apr-2024, QC No. JAA-24-30353; **Revised:** 22-Apr-2024, Manuscript No. JAA-24-30353 (R); **Published:** 21-Mar-2024, DOI: 10.35248/1948-5964.25.17357

Citation: Harrod R, Bowley T, Malu A, Adams NM, Savage J, Saberi M, et al. (2025) The HTLV-1 Latency-Maintenance Factor p30II Induces the Phosphorylation and Hypoxia-Independent Mitochondrial Targeting of TIGAR Analogous to Tyrosine Kinase Receptor-Signaling and Suppresses Oncogene-Induced Oxidative Toxicity. J Antivir Antiretrovir. 17357

drug use/needle sharing, or the transfusion of contaminated blood or blood products [2,7,8]. The development of HTLV-1-associated neoplastic disease (myelodysplastic syndrome or ATLL) results in ~3%-5% of infected individuals, usually following a prolonged latency period of 30-40 years, and can progress into the tertiary form of disease: Acute T-cell leukemia or non-Hodgkin's T-cell lymphoma, which are associated with secondary metastasis (to the bone, liver, spleen and other lymphoid tissues, or CNS), hypercalcemia, osteolytic lesions, and generally poor clinical prognoses [2,3,8].

The HTLV-1 has a complex proviral genome that encodes several regulatory products from alternatively-spliced transcripts, including the major viral transactivator TaxIV, RexIII, p8I, p12I, p13II, p30II, and an antisense-encoded basic domain/leucine zipper protein HBZ, from a highly conserved 3' nucleotide sequence, known as the pX region. The HBZ, p13II, and p30II proteins have all been shown to inhibit Tax-dependent LTR transactivation, viral replication, and suppress the expression of HTLV-1 antigens, albeit through different mechanisms, and are considered to be latency-maintenance factors [1,9-16]. The mRNA transcripts for the pX-ORF-I (p8I/p12I) and ORF-II (p13II/p30II) gene products were detected in freshly isolated lymphocytes from HTLV-1-infected individuals, as well as in HTLV-1+ cell-lines derived from patients with ATLL and HAM/TSP [17,18]. Furthermore, studies using rabbit and rhesus macaque models of HTLV-1 infection have demonstrated that the p13II and p30II products are important for the survival of infected cells and maintenance of a high proviral titer *in vivo* [19-21]. Consistent with their roles in latency-maintenance for the establishment of persistent infections, Pique have isolated cytotoxic T-lymphocytes specific for the pX ORF-II products (p13II/p30II) from HTLV-1-infected asymptomatic carriers and HAM/TSP patients, indicating these pX-II proteins are chronically expressed throughout infection [22]. It is likely that p30II (and p13II) functionally cooperate with other viral proteins, such as Tax and/or HBZ, and modulate their molecular interactions with host cellular components during retroviral pathogenesis.

Although the HTLV-1 transactivator protein Tax has been shown to phosphorylate and stabilize the *p53* tumor suppressor and inhibit *p53*-dependent apoptosis, the *p53* gene is infrequently mutated in most HTLV-1+ ATLL clinical isolates and Zane have demonstrated that wild-type *p53* functions and the Wip1 phosphatase are required for Tax-dependent tumorigenesis *in vivo* in transgenic mice [23,24]. Similarly, we have demonstrated that the HTLV-1 p30II protein inhibits the TIP60-mediated acetylation of *p53* on lysine residue K120 and transactivates the expression of *p53*-regulated pro-survival genes, including tigar [25]. The TIGAR is a 2.6-bis-fructose-phosphatase that localizes to the outer membranes of mitochondria and suppresses the accumulation of Reactive Oxygen Species (ROS) associated with activation of the Myc protooncogene [26-29]. *P53* is a downstream target of Myc and aberrant oncogenic activation of c-Myc induces genomic instability, *p53*-dependent oxidative DNA-damage, and cellular apoptosis [30-36]. Our earlier studies have further demonstrated that p30II activates TIGAR and functionally cooperates with c-Myc (as well as with the other viral oncoproteins Tax and HBZ) and enhances its oncogenic transforming potential in foci-formation assays by inhibiting oncogene-induced oxidative stress and genotoxicity [25,37]. Whereas Cheung, et al., have reported that TIGAR localizes to mitochondrial membranes under hypoxic conditions (0.1% vol/vol O_2) through a mechanism requiring the activation of Hypoxia-Inducible Factor-1 Alpha (HIF-1α) and molecular interactions with Hexokinase-2 (HK2), we surprisingly discovered that p30II induces hypoxia-independent mitochondrial targeting of the TIGAR protein in lentiviral p30II-transduced cells and HTLV-1 ACH-infected cells grown under normoxic conditions (20% vol/vol O_2) [25,38].

The present study provides new insight into the molecular mechanisms by which p30II induces the mitochondrial targeting of TIGAR and comparatively analyzes the ability of HTLV-1 p30II to suppress c-Myc-induced oxidative toxicity with activation of the Myc protooncogene in proliferating cells. Here, we demonstrate that HTLV-1 p30II induces serine-phosphorylation of the TIGAR protein to promote its hypoxia-independent mitochondrial targeting which helps protect proliferating HTLV-1-infected T-lymphocytes against damaging ROS as a result of increased metabolism. Importantly, these studies have shown that p30II modulates TIGAR's subcellular trafficking and antioxidant functions through a conserved mechanism analogous to cellular tyrosine kinase growth factor-receptor signaling. Lentiviral siRNA-knockdown of TIGAR expression resulted in the accumulation of ROS and cytotoxicity in the HTLV-1+ ATLL SLB1 T-cell line and inhibited lymphomagenesis and CNS metastasis in an *in vivo* NOD/scid xenograft model of HTLV-1-induced T-cell lymphoma, which suggests that targeting TIGAR could be a plausible strategy for antiviral/antiretroviral therapy.

MATERIALS AND METHODS

Cell lines and culture conditions

The HT-1080 fibrosarcoma cell line (CCL-121; ATCC, Manassas, VA) was cultured in collagen-coated plastic tissue culture vessels (Greiner Bio-One, Monroe, NC) in Eagle's Minimum Essential Medium (EMEM; ATCC), supplemented with 10% heat-inactivated fetal bovine serum (FBS; Biowest, Bradenton, FL), penicillin (100 U/ml), streptomycin sulfate (100 µg/ml), and gentamycin sulfate (20 µg/ml), at 37°C under 5% CO_2 in a humidified incubator. The A431 squamous carcinoma cell line (CRL-1555; ATCC) was grown in Dulbecco's Modified Eagle's Medium (DMEM; ATCC), supplemented with 10% FBS and antibiotics, at 37°C under 5% CO_2. The 293 Human Embryonic Kidney (HEK) cell line (CRL-1573; ATCC) and 293FT cells (R70007; Invitrogen, Waltham, MA) were cultured in EMEM with 10% FBS and antibiotics and incubated at 37°C and 5% CO_2. The HTLV-1+ MJG11 T-cell line (CRL-8294; ATCC) was cultured in Roswell Park Memorial Institute 1640 (RPMI-1640) Medium (ATCC), supplemented with 20% FBS and antibiotics, at 37°C under 10% CO_2; and the HTLV-1+ SLB1 T-cell line (kindly provided by Dr. P Green, et al the Ohio State University-Comprehensive Cancer Center) and the stable HTLV-1+ SLB1-GFP cell-line were grown in Iscove's Modified Dulbecco's Medium (IMDM) with 10% FBS and antibiotics and incubated at 37°C under 10% CO_2 [39]. The Jurkat E6.1 lymphoblastoid cell line (TIB-152; ATCC) was cultured in RPMI-1640 Medium, supplemented with 10% FBS and antibiotics, at 37°C under 5% CO_2 in a humidified incubator. All cell lines were tested negative for mycoplasma contamination.

Lentiviral packaging and transduction

The lentiviral-HTLV-1 p30II-GFP, lentiviral-siRNA-tigar, and pLenti-6.2/V5-DEST empty vector were packaged to generate infectious VSV-G-pseudotyped virus particles by cotransfecting the lentiviral expression constructs, together with the packaging mix plasmids (pLP1, pLP2, pLP/VSV-G; Invitrogen), into 293FT HEK cells using the Lipofectamine 2000 transfection reagent (Invitrogen) per the manufacturer's recommended protocol. The cultures were monitored for the production of syncytia over four days and then the cells were pelleted by centrifugation at 260 x g at room temperature for 7 minutes and the virus-containing supernatants were collected, clarified by centrifugation, and filtered through

a 0.22 μm polyethersulfone filter. The pseudo typed lentiviral particles were concentrated by ultracentrifugation at 181,866 x g and 4˚C for 24 hours on a 20% (w/v) sucrose-TSE (10 mM Tris (pH 7.5), 100 mM NaCl, 10 mM EDTA) cushion using a Beckman 70.1 Ti rotor. The pelleted lentiviruses were resuspended in TNE (10 mM Tris (pH 7.4), 100 mM NaCl, 1 mM EDTA) buffer and stored in frozen aliquots at -80˚C until ready for use.

HT-1080 fibrosarcoma cells were transduced on 8-chamber Nunc Permanox culture slides (ThermoFisher Scientific, Waltham, MA) with lentiviral-HTLV-1 p30II-GFP or an empty pLenti-6.2/V5-DEST vector as negative control, labeled with the MitoTracker Orange (Molecular Probes, Waltham, MA) mitochondrial probe, and then fixed and stained with a rabbit polyclonal Anti-TIGAR primary antibody (Santa Cruz Biotechnology, Dallas, TX) and Alexa Fluor 488-conjugated donkey Anti-Rabbit IgG fluorescent secondary antibody (Jackson Immunoresearch Laboratories, West Grove, PA) and the samples were subsequently analyzed by confocal microscopy to visualize and quantify the colocalization of the TIGAR protein in mitochondrial structures. To determine the effects of inhibiting TIGAR expression upon intracellular ROS production and *in vivo* tumorigenesis and metastasis, the HTLV-1 SLB1 and HTLV-1 SLB1-GFP T-cell-lines were transduced with either lentiviral-siRNA-tigar to knockdown TIGAR protein levels or an empty pLenti-6.2/V5-DEST vector control. The siRNA-inhibition of TIGAR protein expression was confirmed by Sodium Dodecyl-Sulfate Polyacrylamide Gel Electrophoresis (SDS-PAGE) and immunoblot analysis.

Plasmids, transfections, and antibodies

The following plasmids and expression constructs were used for these experiments: pEGFP-N3-HTLV-1 p30II-GFP, CβF-c-Myc (FLAG-tagged), CβS vector, pLenti-HTLV-1 p30II-GFP, pLenti-siRNA-tigar, and pLenti-6.2/V5-DEST empty vector (Invitrogen) [15,25,40,41]. All plasmid DNA transfections were performed using either Lipofectamine LTX with Plus Reagent or Lipofectamine 2000 transfection reagent (Invitrogen) per the manufacturer's recommended protocols.

The antibodies used for these studies were: Rabbit polyclonal Anti-TIGAR (M-209; Santa Cruz Biotechnology), mouse monoclonal Anti-TIGAR (F-5; Santa Cruz Biotechnology), rabbit polyclonal Anti-Beta Actin (Abcam, Cambridge, UK), goat polyclonal Anti-Beta Actin (C-11; Santa Cruz Biotechnology), mouse monoclonal Anti-Alpha Tubulin (TU-02; Santa Cruz Biotechnology), Rabbit Polyclonal Anti-GFP (FL; Santa Cruz Biotechnology), mouse monoclonal Anti-Phospho-threonine, mouse monoclonal Anti-Phospho-serine, mouse monoclonal Anti-Phospho-tyrosine (Millipore-Sigma, St. Louis, MO), rabbit monoclonal Anti-TOMM20 (EPR15581-54; Abcam), rabbit monoclonal Anti-IkB alpha (E130; Abcam), mouse monoclonal Anti-c-Myc (9E10; Millipore-Sigma), mouse monoclonal Anti-FLAG M2 (Millipore-Sigma), mouse monoclonal Anti-Acetyl-K120-*p53* (10E5; Abcam), rabbit monoclonal Anti-Acetyl-K373-*p53* (EP356(2)AY; Abcam), rabbit polyclonal Anti-*p53* (FL-393; Santa Cruz Biotechnology), mouse monoclonal Anti-*p53* (DO-2; Santa Cruz Biotechnology), Alexa Fluor 488-conjugated donkey Anti-Rabbit IgG (H+L) fluorescent secondary antibody, Alexa Fluor 488-conjugated donkey Anti-Mouse IgG (H+L) fluorescent secondary antibody, Rhodamine (TRITC)-conjugated donkey Anti-Rabbit IgG (H+L) fluorescent secondary antibody, Peroxidase-conjugated donkey Anti-Mouse IgG (H+L) secondary antibody, Peroxidase-conjugated donkey Anti-Goat IgG (H+L), and Peroxidase-conjugated goat Anti-Rabbit IgG (H+L) secondary antibody (Jackson Immunoresearch Laboratories).

Immunoprecipitations and western blotting

To detect the expression of individual proteins and posttranslational modifications by immunoprecipitations, the cultured cells were harvested and pelleted by centrifugation at 260 x g at 4˚C for 7 min and then the samples were resuspended in 500 μl of RIPA buffer (0.15 M NaCl, 50 mM Tris-Cl, pH 7.4, 0.5% sodium deoxycholate, 0.5% Nonidet P-40, 0.1% Sodium Dodecyl Sulfate (SDS)) containing 50 ng/ml each of the protease inhibitors: Pepstatin, leupeptin, chymostatin, bestatin, and antipain-dihydrochloride (Roche Molecular Diagnostics, Pleasanton, CA). The samples were lysed by repeated freeze-thawing and passaging through a 27-gauge tuberculin syringe, or sonication over an ice-bath using a Misonix S-4000 model instrument and microtip probe (Cole Parmer, Vernon Hills, IL) set at 70% amplitude. Alternatively, mitochondrial and cytoplasmic fractions were prepared by harvesting and centrifuging the cells at 260 x g at 4˚C for 10 min. The mitochondria were isolated using a Qproteome Mitochondria Isolation kit (Qiagen, Germantown, MD) per the manufacturer's recommended protocol. The cells were lysed by sonication, clarified by centrifugation at 1200 x g at 4˚C for 10 min, and then the supernatants were transferred to new 1.5 ml microtubes. The samples were centrifuged again at 6400 x g at 4˚C for 10 min and the microsomal fractions were transferred to separate 1.5 ml microtubes. The mitochondrial pellets were resuspended in 1 ml of ice-cold Mitochondrial Storage Buffer (Qiagen) and washed by centrifugation at 6400 x g at 4˚C for 20 min and resuspended in 100 μl of Mitochondrial Storage Buffer (Qiagen) for subsequent analysis. The purity of the isolated mitochondrial and cytoplasmic fractions was confirmed by performing denaturing SDS-PAGE, followed by Western blotting with primary antibodies to detect the mitochondrial membraneprotein (TOM20) and IκB-α as a cytoplasmic marker. Immunoprecipitations were carried out by lysing the cells in 500 μl of RIPA buffer (0.15 M NaCl, 50 mM Tris-HCl, pH 7.4, 0.5% sodium deoxycholate, 0.5% Nonidet P-40, 0.1% SDS) containing protease inhibitors. The samples (250 μl) were mixed with 20 μl of a 50% slurry of Protein-G agarose beads (Invitrogen) and 3 μl-5 μl of the antibodies and incubated overnight at 4˚C with gentle rotation. The bound complexes were then pelleted by centrifugation at 5000 x g at 4˚C for 5 min, washed 2X with RIPA buffer, and resuspended in 30 μl of 2X Laemmli Sample Buffer with 2-mercaptoethanol (Biorad Laboratories, Hercules, CA). The samples were denatured by heating at 95˚C for 5 min and then briefly centrifuged at 10000 x g for 2 min. The cellular proteins were subsequently resolved by SDS-PAGE on a 12.5% polyacrylamide gel with a 4% stacking layer and electrophoresed using a 0.025 M Tris-0.19M glycine, pH 8.3, running buffer. The proteins were transferred for 1 hr onto a Protran BA83 0.2 mm nitrocellulose membrane (Whatman, Maidstone, UK) using a model 77 PWR semi-dry unit (Amersham Biosciences, Little Chalfont, UK) and Tris-glycine Transfer Buffer (48 mM Tris base, 39 mM glycine, 0.037% (w/v) SDS, 20% (v/v) methanol). Western blotting was performed by blocking the membranes for 1 hr at room temp with gentle agitation in BSA Blocking Buffer 3% (w/v) bovine serum albumin and 0.5% (v/v) Tween-20 in phosphate buffered saline, PBS, pH 7.4). The membranes were then incubated with primary antibodies (diluted 1:1000) in BLOTTO Buffer (50 mM Tris-HCl, pH 8.0, 2 mM $CaCl_2$, 80 mM

NaCl, 0.2% (v/v)) IGEPAL-CA630, 0.02% (w/v) sodium azide, and 5% (w/v) nonfat dry milk) for 2 hours with gentle agitation. The membranes were then washed 2X with BLOTTO Buffer for 10 minutes and incubated with appropriate Peroxidase-conjugated secondary antibodies (diluted 1:500 in BLOTTO) for another 1.5 hours on an orbital shaker. The samples were later washed 2X with BLOTTO Buffer and once with TMN Buffer (100 mM Tris-HCl, pH 9.5, 5 mM MgCl2, 100 mM NaCl) for 10 min each, and the membranes were developed by chemiluminescence imaging using Pierce ECL Western Blot Reagent (ThermoFisher Scientific) and a ChemiDoc Touch imaging system with densitometry quantitation of the protein bands using Image Lab 6.0.1 software (Biorad Laboratories). For the mitochondrial and cytoplasmic fractions, the phosphorylated TIGAR protein was immunoprecipitated using monoclonal Anti-Phospho-Serine or Anti-Phospho-Tyrosine (as a negative control) antibodies and the relative Mit/Cyt Phospho-Ser Indices were calculated by dividing the ratio of mitochondrial phospho-Ser: phospho-Tyr by the ratio of cytoplasmic phospho-Ser: Phospho-Tyr signals.

For the *in vivo* tumorigenesis experiments, the HTLV-1+ SLB1 ATLL cell-line was transduced with either lentiviral-siRNA-tigar to knockdown TIGAR protein expression, or an empty pLenti vector as negative control. The cells were harvested and pelleted by centrifugation at 260 x g at 4˚C for 7 minutes, then the samples were resuspended in 100 µl of 1x Lysis Buffer (Promega, Madison, WI) and lysed by sonication over an ice-bath, followed by repeated freeze-thawing. The samples were clarified by centrifugation at 5000 x g for 5 minutes at 4˚C and subsequently analyzed by SDS-PAGE and immunoblotting. The inhibition of TIGAR protein expression was demonstrated using rabbit polyclonal Anti-TIGAR and goat polyclonal Anti-Beta Actin primary antibodies (diluted 1:1000) and appropriate Peroxidase-conjugated secondary antibodies (diluted 1:500). The immunoblot signals were detected using chemiluminescent imaging, quantified by densitometry, and normalized relative to Actin protein levels.

Measuring intracellular ROS

The effects of inhibiting TIGAR upon the accumulation of damaging Reactive Oxygen Species (ROS) were determined by plating HTLV-1+ SLB1 T-lymphoblasts on an 8-chamber tissue-culture slide and then transducing them with either an empty lentiviral vector or a lentiviral-siRNA-tigar expression construct to knockdown TIGAR protein expression. The samples were stained with the ROS-specific fluorescent chemical probe, 5-(and-6)-chloromethyl-2',7'-dichlorodihydrofluorescein diacetate, acetyl ester (CM-H2DCFDA, 2.5 µM; Invitrogen), rinsed 3X with PBS, pH 7.4, and fixed for 15 minutes at room temp in a solution of 2% formaldehyde/0.2% glutaraldehyde/PBS. After fixation, the solution was removed and the slides were washed 3X with PBS, pH 7.4, and then fluorescence mounting medium (KPL) and glass coverslips were added. The samples were analyzed by confocal microscopy and the relative percentages of ROS (CM-H2DCFDA)-positive cells were quantified by counting each visual field in-triplicate at 200X magnification.

In vivo tumorigenesis and CNS metastasis

To determine if the siRNA-inhibition of TIGAR might influence *in vivo* tumorigenesis by HTLV-1, immunodeficient NOD/scid mice (Charles River Laboratories, Wilmington, MA) were anesthetized by gas inhalation of 3%-5% isoflurane/O_2 and then intraperitoneally engrafted with 1 x 106 of a stable HTLV-1+ SLB1-Green Fluorescent Protein (SLB1-GFP) cell-line that had been previously transduced with a either lentiviral-siRNA-tigar expression vector or an empty pLenti vector control using a sterile 27-gauge tuberculin syringe. For comparison, another group of animals was injected with the Vehicle alone (i.e., sterile Ca^{2+}/Mg^{2+}-free PBS, pH 7.4) as a negative control [39]. The experimental animals (n=3 per sample group) were monitored daily for any changes to their overall health status (signs of lethargy, morbidity, rough fur, pain, discomfort, or difficulty eating, drinking, or with ambulation) or abdominal distension associated with HTLV-1-induced lymphomagenesis. After 10-12 weeks, the animals were humanely sacrificed and the tumor tissues and any affected secondary organs (e.g., spleen, pancreas, liver, and brain) were harvested, weighed and measured using a digital caliper. The tumor volumes were determined using the calculation: (D x d2)/2, where 'D' equals the longest diameter and 'd' equals the shortest diameter. The tissues were fixed in 10% neutral-buffered formalin (3.75% formaldehyde, 33.3 mM sodium phosphate monobasic, 45.8 mM sodium phosphate dibasic, in distilled deionized water, pH 6.8), embedded in Histoplast IM paraffin (ThermoFisher Scientific) blocks, and then processed and sectioned using a Microm HM360 rotary microtome for analysis by confocal microscopy. The *in vivo* xenograft studies of HTLV-1 tumorigenesis were performed in accordance with protocol No. A16-001-HARR which was approved by the Southern Methodist University-Institutional Animal Care & Use Committee.

Microscopy and confocal imaging

Confocal imaging was performed on a Zeiss LSM800 inverted microscope system with an Airyscan super-resolution detector and using either a Plan-Apochromat 20X/0.8 objective, or Plan-Apochromat 40X/1.3 or 63X/1.4 oil immersion objectives (Carl Zeiss Microscopy, Gottingen, Germany). The colocalization between TIGAR and the fluorescent MitoTracker Orange probe or the mitochondrial membrane protein TOM20 was quantified across a randomly positioned 5 µm square area using the ZEN OS-Colocalization module and Pearson correlation coefficient (Carl Zeiss Microscopy). The expression of lentiviral-HTLV-1 p30II-GFP was visualized by fluorescence microscopy using an inverted Nikon Eclipse TE2000-U microscope and D-Eclipse C1 confocal system equipped with 633 nm and 543 nm He/Ne lasers and 488 nm Ar lasers and using a Plan-Apochromat 20X/0.75 objective lens (Nikon Instruments, Melville, NY). The tumor tissues and affected secondary organs from *in vivo* HTLV-1 tumorigenesis experiments were imaged using a Zeiss Discovery.V8 stereomicroscope equipped with an AxioCam HRc color camera (Carl Zeiss Microscopy).

Data analysis

The statistical significance of experimental data sets was determined using unpaired two-tailed Student's t-tests (alpha=0.05) and calculated P-values using GraphPad Prism 8.0 software (GraphPad Software, San Diego, CA), with the P-values defined as: 0.1234 (ns), 0.0332 (*), 0.0021 (**), 0.0002 (***), <0.0001 (****). NCSS PASS 2020 sample-size statistical software (NCSS Statistical Software LLC, Kaysville, UT) was used for the power determinations for *in vivo* studies. All experiments were performed at least three times (N-value ≥ 3) with the exception of the *in vivo* xenograft tumorigenesis studies in NOD/scid mice which used three animals per sample group.

RESULTS

HTLV-1 p30II induces serine-phosphorylation of the TIGAR protein associated with its hypoxia-independent mitochondrial targeting.

The expression of TIGAR is regulated by *p53*, TAp63, TAp73, NRF2, SP1, CREB, and/or Myc-dependent transcriptional activation [26-29,42-46]. Our earlier studies have demonstrated that the HTLV-1 latency protein p30II interacts with the MYST-family acetyltransferase TIP60 (a cofactor for both Myc and *p53*) [47-57]; and inhibits TIP60-mediated *p53*-K120-acetylation, prevents *p53*-dependent apoptosis, and activates Myc and *p53*-dependent transcription, including tigar gene expression in HTLV-1-transformed ATLL cells [25,37,47,58]. Whereas others have shown that a significant fraction of the TIGAR protein translocates from the cytoplasm to the outer membranes of mitochondria under conditions of hypoxia or ischemic injury, which requires HIF-1α activation and molecular interactions with HK2 [26-28,38,59,60], we have previously demonstrated that the viral p30II protein induces hypoxia-independent mitochondrial targeting of TIGAR which protects HTLV-1-infected cells against oncogene (i.e., Tax, HBZ, and c-Myc)-induced oxidative genotoxicity [25,37,58]. These findings were reproduced in HT-1080 cells (which contain wild-type *p53* and inducible tigar expression); that were transduced with a lentiviral-HTLV-1 p30II-Green Fluorescent Protein (p30II-GFP) expression vector [25,37]. These cells have a higher cytoplasmic-to-nuclear ratio which facilitates easier visualization of mitochondrial structures (in contrast to lymphoid cells). The results in Figures 1A and 1B demonstrate that the TIGAR protein colocalized with the mitochondria-specific fluorescent probe, MitoTracker Orange (Invitrogen), in lentiviral-HTLV-1 p30II-GFP transduced cells as determined by immunofluorescence-confocal microscopy. Importantly, the molecular mechanisms by which p30II promotes the intracellular trafficking and mitochondrial targeting of TIGAR remains to be fully elucidated. We therefore investigated whether p30II could induce posttranslational phosphorylation of the TIGAR protein. As shown in Figure 1C, the lentiviral-HTLV-1 p30II-GFP induced the expression of TIGAR in transduced cells, as compared to the empty lentiviral vector control (Input lanes). Using a panel of phospho-specific monoclonal antibodies, the phosphorylated TIGAR protein was immune precipitated with Protein-G agarose beads and then detected by Western blotting. Surprisingly, these experiments revealed that HTLV-1 p30II specifically induces serine-phosphorylation, but not threonine-or tyrosine-phosphorylation, of the TIGAR protein (Figure 1C). To confirm these results and delineate the p30II-responsive signaling pathway(s) that may be involved, we examined the effects of various chemical kinase-inhibitors (i.e., wortmannin, staurosporine, and SB203580) upon p30II-induced TIGAR phosphorylation. As shown in Figure 1D, the p30II-GFP induced the expression and serine-phosphorylation of the TIGAR protein in transfected cells, as compared to an empty vector control (Input lanes). However, the chemical inhibitor, wortmannin (a broad-specificity inhibitor of phosphatidylinositol-3-kinase, PI3K), but neither staurosporine (an inhibitor of protein kinase C and other calcium-dependent kinases) nor SB203580 (a p38MAPK inhibitor), effectively blocked the serine-phosphorylation of TIGAR by the HTLV-1 p30II protein (Figure 1D). Based upon these findings, we next sought to determine if phosphorylation regulates the hypoxia-independent mitochondrial targeting of TIGAR by the viral p30II protein. For these experiments, HT-1080 cells were transduced with lentiviral-HTLV-1 p30II-GFP or an empty lentiviral vector as negative control, and mitochondrial and cytoplasmic fractions were prepared using a Qproteome Mitochondria Isolation kit (Qiagen). The expression of p30II-GFP was visualized by fluorescence-microscopy (Figure 1E)-micrograph. The expression and subcellular distribution of TIGAR were analyzed by immunoblotting; and the purity of mitochondrial fractions was confirmed using the outer membrane protein, TOM20, as a mitochondrial marker and the Inhibitor of kappa B-alpha (IκB-α) as an indicator of the cytoplasmic fractions (Figure 1E). Consistent with our previous observations, the levels of TIGAR were markedly induced in p30II-GFP expressing cells with a significant portion targeted to the mitochondrial fraction (Figure 1E). Immunoprecipitations were then performed using monoclonal Anti-Phospho-Serine or Anti-Phospho-Tyrosine (as a negative control) antibodies and Protein-G agarose beads and the bound phosphorylated TIGAR protein was detected by immunoblotting. The Mit/Cyt Phospho-Ser Indices were calculated as described in the Materials and methods section. These experiments revealed that HTLV-1 p30II induces the serine-phosphorylation of TIGAR which correlates with its hypoxia-independent targeting to mitochondrial membranes, and further provides mechanistic evidence that posttranslational modifications and phospho-signaling regulate the intracellular trafficking and mitochondrial antioxidant functions of the TIGAR (Figure 1E).

Figures 1A and 1B demonstrates HT-1080 cells were transduced with a lentiviral HTLV-1 p30II-GFP expression construct, labeled with MitoTracker Orange (red signal), and immunofluorescence-confocal microscopy was performed using an Anti-TIGAR primary antibody (green signal). The colocalization between the MitoTracker Orange and TIGAR-specific fluorescent signals was measured using the ZEN OS Colocalization tool (Carl Zeiss Microscopy; n-value=20). The data is mean ± SD; (Figure 1C)-HT-1080 cells were transduced either with lentiviral HTLV-1 p30II-GFP or an empty lentiviral vector as negative control. The expression of the p30II-GFP, TIGAR, and Actin proteins was detected by immunoblotting and the relative levels of TIGAR were quantified by densitometry and normalized relative to Actin (Input panels). Immunoprecipitations were performed using monoclonal phospho-specific antibodies: Anti-Phospho-Serine, Anti-Phospho-Threonine, and Anti-Phospho-Tyrosine (Millipore-Sigma), and Protein-G agarose beads (Invitrogen) and the relative amounts of the precipitated phosphorylated proteins were detected by Western blotting using a polyclonal Anti-TIGAR antibody; (Figure 1D)-The cells were transfected with either CMV-HTLV-1 p30II-GFP or an empty CβS vector as negative control and then the cultures were treated with various chemical kinase inhibitors: wortmannin (20 nM), staurosporine (12.5 nM), or SB203580 (50 nM; Millipore-Sigma). The expression of p30II-GFP and TIGAR was detected by immunoblotting. The relative levels of TIGAR were quantified by densitometry with normalization to Actin (Input panels). Immunoprecipitations were performed using a monoclonal Anti-Phospho-Serine antibody and the precipitated phosphorylated TIGAR protein was detected by immunoblotting. (Figure 1E) HT-1080 cells were transduced with either lentiviral HTLV-1 p30II-GFP or an empty lentiviral vector, lysed by sonication, and isolated mitochondrial and cytoplasmic fractions were prepared using a Qproteome Mitochondria Isolation kit (Qiagen). The expression of TIGAR was detected by immunoblotting; and the purity of the mitochondrial and cytoplasmic fractions was confirmed by detecting the mitochondrial outer membrane protein, TOM20,

and IkB-α as a cytoplasmic marker (Input panels). The HTLV-1 p30II-GFP protein was visualized by fluorescence-microscopy (right). Immunoprecipitations were performed with the isolated mitochondrial and cytoplasmic fractions using monoclonal Anti-Phospho-Serine and Anti-Phospho-Tyrosine (as a negative control) antibodies. The precipitated phosphorylated TIGAR protein (asterisk) was detected by immunoblotting and quantified by densitometry, and the relative Mitochondrial/Cytoplasmic Phospho-Ser Indices were calculated as described in the materials and methods. All the data in Figures 1A-1E is representative of at least three independent experiments (Figure 1).

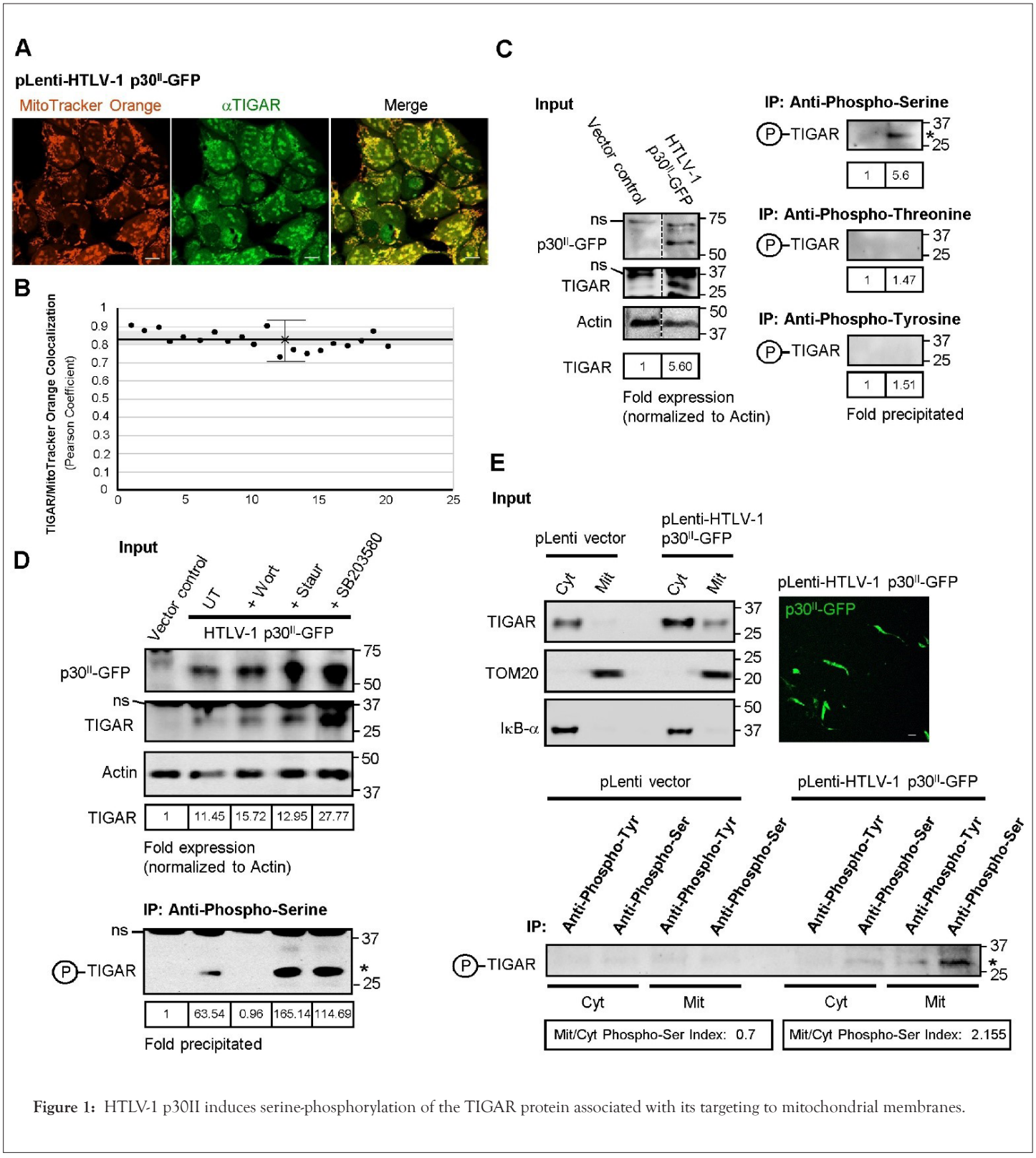

Figure 1: HTLV-1 p30II induces serine-phosphorylation of the TIGAR protein associated with its targeting to mitochondrial membranes.

Tyrosine kinase receptor-signaling activates TIGAR and induces its serine-phosphorylation and mitochondrial targeting associated with Myc-dependent mitogenic functions

The aberrant unscheduled activation of c-Myc proliferative signaling results in oxidative genomic DNA-damage, cellular senescence, and *p53*-dependent apoptosis and is an intrinsic barrier against neoplastic disease [30,34-36,61-64]. Nevertheless, the myc protooncogene is a downstream transcriptional target of many mitogenic/proliferative signaling pathways, including tyrosine kinase growth factor-receptors (e.g., Epidermal Growth Factor-Receptor (EGFR)) [65-68], and Myc induces the entry of cells into the S-phase of the cell-cycle by controlling the expression of cyclin D2 [69-71]. We thus hypothesized the induction of TIGAR by Myc and/or *p53* could counter the oxidative genotoxicity associated with Myc activation and thereby promote the survival of proliferating cells in response to tyrosine kinase-receptor-signaling. Indeed, Cheung et al., have demonstrated that Wnt/Beta-catenin-signaling induces tigar gene expression through Myc activation in an APC-deleted *in vivo* model of intestinal carcinogenesis; and that c-Myc also upregulates TIGAR in a transgenic Eμ-Myc mouse model of B-cell lymphoma where c-Myc expression is driven by an IgH promoter [29]. Inhibitors of the tyrosine kinase-receptor, c-Met, have been shown to downregulate TIGAR expression in nasopharyngeal carcinomas; and TIGAR induces the Epithelial-To-Mesenchymal Transition (EMT) and tumor cell invasiveness by Hepatocyte Growth Factor (HGF, or scatter factor)/Met receptor-signaling in non-small-cell lung cancers [72,73]. We first analyzed the expression of TIGAR and Myc by immunoblotting over a time-course in A431 squamous carcinoma cells that were stimulated *in vitro* with recombinant human EGF (hEGF, 2 μg/ml). The results in Figure 2A (Input lanes) demonstrate that the TIGAR protein was rapidly induced associated with Myc activation in hEGF-stimulated cells. Immunoprecipitations of these cell extracts using various phospho-specific monoclonal antibodies revealed that TIGAR is strongly phosphorylated on serine residues, but not on threonine or tyrosine, in response to EGFR signaling (Figure 2A). To determine if tyrosine kinase-receptor signaling induces serine-phosphorylation of the TIGAR protein associated with its translocation to mitochondrial membranes, 293 HEK cells were treated with recombinant hEGF for 2 hours and then mitochondrial and cytoplasmic fractions were prepared using a Qproteome Mitochondria Isolation kit. The purity of the fractions was confirmed by immunoblotting to detect the mitochondrial marker, TOM20, and the cytoplasmic protein, IκB-α (Figure 2B). These studies demonstrated that the TIGAR protein significantly localizes to mitochondrial membranes in response to tyrosine kinase-receptor signaling (Figure 2B), input lanes; see Overexposed immunoblot). We next performed immunoprecipitations on the isolated fractions and found that the TIGAR protein was strongly phosphorylated on serine residues in the mitochondrial fraction from hEGF-stimulated cells, but not Untreated (UT) cells (Figure 2B). To determine which kinase signaling pathways may be involved in the EGF-induced hypoxia-independent mitochondrial targeting of TIGAR, 293 HEK cells were stimulated with hEGF for 2 hours, either in the absence or presence of various chemical kinase inhibitors (i.e., wortmannin, staurosporine, or SB203580), and the serine-phosphorylated TIGAR was then analyzed by immunoprecipitation and Western blotting with densitometric quantitation. The results in Figure 2C demonstrate that the TIGAR protein was phosphorylated on serine residues in the +hEGF/Control sample and this was not significantly diminished in the +hEGF/Staur or +hEGF/SB203580 samples. We also observed that expression of the TIGAR protein was increased in growth factor-stimulated cells. However, wortmannin-treatment markedly inhibited the serine-phosphorylation of TIGAR in response to EGF-receptor signaling (Figure 2C). These findings were further validated by immunofluorescence-confocal microscopy analysis which demonstrated the stimulation of cells with hEGF resulted in the hypoxia-independent mitochondrial targeting of TIGAR within 1-2 hours (Figures 2D and 2E). Mitochondrial structures were labeled using a primary antibody that recognizes TOM20 (red signal in micrographs); and the colocalization of the TIGAR-specific (green) fluorescent signal with TOM20 resulted in a yellowish fluorescent signal in the Anti-TOM20/TIGAR merged images (Figure 2D). The colocalization between the TIGAR/TOM20-specific fluorescent signals was measured across a randomly positioned 5μm^2 area using the Carl Zeiss Microscopy-Zen OS Colocalization module and the Pearson colocalization coefficient (Figure 2E). The results shown in Figures 2F and 2G demonstrate that, although TIGAR strongly colocalized with the TOM20-mitochondrial signal in hEGF-stimulated cells that were treated with staurosporine, the chemical kinase inhibitor wortmannin effectively blocked the mitochondrial localization of TIGAR in +hEGF/Wortmannin treated cells (Figures 2F and 2G). These data collectively suggest that both HTLV-1 p30II and tyrosine kinase-receptor (hEGFR) signaling induce serine-phosphorylation and hypoxia-independent mitochondrial targeting of the TIGAR protein, possibly through a conserved mechanism, associated with Myc-dependent mitogenic activation in proliferating cells.

Figure 2A demonstrates A431 squamous carcinoma cells were stimulated with human recombinant EGF (hEGF, 2 μg/ml; Roche Applied Science) in complete growth medium over a 12 hr time-course. At regular intervals, the cells were harvested and lysed in RIPA buffer and the expression of TIGAR and Myc was detected by immunoblotting and quantified by densitometry with normalization to Actin (Input panels). Immunoprecipitations were performed using various monoclonal phospho-specific antibodies (i.e., Anti-Phospho-Serine, Anti-Phospho-Threonine, and Anti-Phospho-Tyrosine) and Protein-G agarose beads, and the precipitated phosphorylated TIGAR protein (asterisk) was detected by Western blotting. (Figure 2B)-293 HEK cells were stimulated with hEGF (2 μg/ml) for 2 hr and then subsequently lysed by sonication over an ice-bath, and mitochondrial and cytoplasmic fractions were prepared using a Qproteome Mitochondria Isolation kit. The purity of the isolated fractions was confirmed by immunoblotting to detect TOM20 and IkB-β. The expression of TIGAR was detected by immunoblotting (the overexposed image shows increased TIGAR present in the mitochondrial fraction of hEGF-stimulated cells). Immunoprecipitations were performed using Anti-Phospho-Serine and Anti-Phospho-Tyrosine (as a negative control) antibodies and Protein-G agarose beads and the relative levels of precipitated phosphorylated TIGAR (asterisk) were detected by immunoblotting and the Mitochondrial/Cytoplasmic Phospho-Ser Indices were calculated. (Figure 1C)-293 HEK cells were stimulated with hEGF for 2 hr in the absence or presence of various chemical kinase inhibitors: wortmannin (20 nM), staurosporine (12.5 nM), or SB203580 (50 nM), and the expression of TIGAR was detected by immunoblotting and quantified with normalization to Actin protein levels (Input panels). Immunoprecipitations were performed using a monoclonal Anti-Phospho-Serine antibody and the relative

amounts of precipitated phosphorylated TIGAR were detected by Western blotting and quantified with densitometry. (Figures 2D and 2E)-293 HEK cells were stimulated with hEGF (2 μg/ml) over a 12 hr time-course and the mitochondrial targeting of the TIGAR protein was visualized by immunofluorescence-confocal microscopy using rabbit monoclonal Anti-TOMM20 (red signal) and mouse monoclonal Anti-TIGAR (green signal) primary antibodies and appropriate fluorescent secondary antibodies. Scale bar, 20 μm. The colocalization between the TOM20 and TIGAR-specific fluorescent signals was measured using the ZEN OS Colocalization tool. Twenty individual cells were quantified for each data point (n-value=20). (Figures 2F and G)-293 HEK cells were stimulated with hEGF for 2 hr in the absence or presence of various chemical kinase inhibitors as in C, and immunofluorescence-confocal microscopy was performed to visualize the colocalization between the TIGAR (green signal) and TOM20 (red signal) proteins. Twenty individual cells were quantified for each data point (n-value=20). The asterisks denote statistical significance as determined using unpaired two-tailed Student's t-tests (**P<0.0021). All the data in A-G is representative of at least three independent experiments (Figure 2).

Both HTLV-1 p30II and tyrosine kinase growth factor-receptor signaling inhibit K120-acetylation of the TP53 protein and induce TP53-K373-acetylation

Aberrant c-Myc oncogenic expression can activate the *p53* tumor suppressor (through E-box enhancer elements within the *p53* gene promoter and stabilization of the *p53* protein by p14ARF (or p19ARF in mice); and induce oxidative DNA-damage, genotoxicity, and *p53*-dependent cellular apoptosis [30-36,61-64,74-77]. Several studies have demonstrated the acetylation of *p53* on lysine residue K120 by TIP60 (or Kat5) differentially modulates the expression of *p53*-regulated pro-apoptotic genes; and the TIP60 acetyltransferase mediates the c-Myc oncogene-induced DNA-damage response [51,54,56,57,61,78-80]. Conversely, the *p53* tumor suppressor is acetylated on lysine residues K320 and K373/K382 by PCAF and p300, respectively, and mediates the expression of *p53*-dependent cell-cycle checkpoint regulators and growth-arrest genes, including p21Waf1/Cip1 and gadd45 [81-83]. We therefore next sought to determine if Myc proto-oncogene activation and the induction of mitochondrial TIGAR by tyrosine kinase-receptor signaling or the HTLV-1 p30II protein are associated with differential posttranslational modifications of the *p53* tumor suppressor. 293 HEK cells were stimulated *in vitro* for 2 hrs or 4 hrs with hEGF and then the expression of Myc and *p53* was analyzed by immunoblotting and densitometric quantitation. The results in Figure 3A (Input lanes) demonstrate that the expression of these factors was increased in the hEGF-stimulated cells, as compared to untreated control cells. The K120-acetylated and K373-acetylated *p53* proteins were immunoprecipitated from extracts prepared form these cells and, as shown in Figure 3A (IP lanes), Tyrosine Kinase-Receptor (EGF-R) mitogenic signaling resulted in robust *p53*-K373-acetylation but did not induce *p53*-K120-acetylation which is associated with cellular apoptosis [51,52]. We then compared the effects of the HTLV-1 p30II protein upon c-Myc-induced *p53*-acetylation in transfected cells. Consistent with oxidative genotoxicity and a *p53*-dependent DNA-damage response induced by aberrant c-Myc oncogenic expression, the overexpression of c-Myc resulted in higher levels of *p53*-K120-acetylation as compared to untreated cells (Figure 3B). Surprisingly, HTLV-1 p30II-GFP increased the expression of the TIGAR protein in c-Myc-expressing cells which correlated with the induction of p53-K373-acetylation and the inhibition of c-Myc-dependent p53-K120-acetylation (Figure 3B). These results suggest that tyrosine kinase-receptor signaling and the HTLV-1 p30II protein similarly induce p53-K373-acetylation by p300 and inhibit TIP60-mediated p53-K120-acetylation, associated with the induction of TIGAR, to promote Myc proto-oncogene activation and counter oncogene-induced cytotoxicity in proliferating cells.

Figure 3A demonstrates 293 HEK cells were plated with serum-starvation (i.e., 0.05% FBS) overnight and then stimulated with hEGF (2 μg/ml) in complete medium for either 2 hr or 4 hr. Untreated (UT) cells are shown for comparison. The cells were subsequently harvested by scraping, lysed in RIPA buffer, and the relative expression of the TIGAR, Myc, and *p53* proteins was detected by immunoblotting and quantified by densitometry with normalization to Tubulin (Input panels). Immunoprecipitations were performed using mouse monoclonal Anti-Acetyl-K120-*p53* (10E5) and rabbit monoclonal Anti-Acetyl-K373-*p53* (EP356(2) AY) antibodies (Abcam) and Protein-G agarose beads and the bound acetylated *p53* protein was detected by immunoblotting with densitometric quantitation. (Figure 3B)-293 HEK cells were co-transfected with CβF-c-Myc (FLAG-tagged) and either CMV-HTLV-1 p30II-GFP or an empty CβS vector as negative control, and the relative expression of TIGAR and *p53* was detected by immunoblotting and quantified with normalization for Tubulin. The FLAG-tagged c-Myc oncoprotein and HTLV-1 p30II-GFP were also detected by immunoblotting (Input panels). Immunoprecipitations were performed using Anti-Acetyl-K120-*p53* and Anti-Acetyl-K373-*p53* antibodies as described in A and the acetylated *p53* protein was detected by Western blotting. All the data in A and B is representative of at least three independent experiments (Figure 3).

The TIGAR protein is serine-phosphorylated associated with its mitochondrial targeting in HTLV-1-transformed ATLL lymphoblasts

We next investigated whether the TIGAR protein is phosphorylated on serine-residues associated with its mitochondrial localization in HTLV-1-transformed ATLL T-cell-lines (SLB1 and MJG11), as compared to HTLV-1-negative Jurkat E6.1 lymphoblasts. As shown in Figure 4A (Input lanes) and consistent with our previous reports, the TIGAR was significantly upregulated in HTLV-1+ ATLL lymphocytes compared to the negative control Jurkat T-cells [25,37]. Also, the TIGAR protein was strongly phosphorylated on serine-residues (but not on threonine or tyrosine) in the HTLV-1+ SLB1 and MJG11 ATLL cell-lines, in contrast to the HTLV-1-negative Jurkat cells (Figure 4A). We then prepared mitochondrial and cytoplasmic fractions from the HTLV-1+ ATLL cell-lines (SLB1 and MJG11) using a Qproteome Mitochondria Isolation kit and analyzed the subcellular distribution of the TIGAR protein by immunoblotting. The purity of mitochondrial fractions was confirmed by detecting the outer membrane protein TOM20; and IκB-α was detected as a marker for the cytoplasmic fractions (Figure 4B). In agreement with reports by others, the TIGAR protein was predominantly localized in the cytoplasm with a minor portion targeted to the outer membranes of mitochondria in HTLV-1+ ATLL cells (Figure 4B) [26,27,38]. The phosphorylated TIGAR protein was immunoprecipitated from the isolated cytoplasmic and mitochondrial fractions using Anti-Phospho-Serine and Anti-Phospho-Tyrosine (as a negative control) monoclonal antibodies and Protein-G agarose beads and then detected by

immunoblotting with densitometric quantitation. The results from these experiments demonstrate that the serine-phosphorylation of TIGAR specifically correlated with its localization in mitochondrial fractions (Figure 4B). To further confirm these findings, the subcellular distribution of TIGAR was analyzed in HTLV-1-transformed ATLL cells (MJG11 and SLB1) and HTLV-1-negative Jurkat T-lymphocytes by immunofluorescence-confocal microscopy. The mitochondrial structures in these cells were labeled with MitoTracker Orange (Invitrogen). As depicted in the micrographs in Figure 4C, the TIGAR-specific (green) signal significantly overlapped with the MitoTracker Orange (red) signal and resulted in yellowish colocalization in the merged images, in contrast to Jurkat T-cells which exhibited little TIGAR expression consistent with the immunoblotting results in Figure 4A and produced a more reddish orange color in the merged images. Importantly, the results in Figure 4D demonstrate that the chemical kinase inhibitor wortmannin, but neither staurosporine nor SB203580, inhibited the mitochondrial targeting of TIGAR and colocalization between the TIGAR/MitoTracker Orange fluorescent signals in the HTLV-1-transformed ATLL cell-lines, MJG11 and SLB1, as compared to the Jurkat negative control cells. These findings suggest that the serine-phosphorylation of TIGAR modulates its mitochondrial antioxidant functions and could help protect HTLV-1+ ATLL cells against oncogene-induced oxidative stress and genotoxicity. siRNA-inhibition of TIGAR expression results in the accumulation of cytotoxic ROS in HTLV-1-transformed ATLL T-cells.

Figure 4A demonstrates the expression of TIGAR in the HTLV-1-transformed ATLL T-cell-lines, SLB1 and MJG11, as compared to Jurkat E6.1 lymphocyte was detected by immunoblotting and quantified by densitometry with normalization to Tubulin levels (Input panels). Immunoprecipitations were performed using various phospho-specific monoclonal antibodies: Anti-Phospho-Threonine, Anti-Phospho-Tyrosine, and Anti-Phospho-Serine (Millipore-Sigma) and Protein-G agarose beads (Invitrogen) and the relative amounts of the bound phosphorylated TIGAR protein were analyzed by immunoblotting and quantified with densitometry. (Figure 4B)-Mitochondrial and cytoplasmic extracts were prepared from the HTLV-1-transformed ATLL T-cell-lines, SLB1 and MJG11, using a Qproteome Mitochondria Isolation kit (Qiagen) per the manufacturer's suggested protocol. The purity of the isolated fractions was confirmed by performing Western blots to detect the mitochondrial outer membrane protein, TOM20, and IkB-α as a cytoplasmic marker. The input levels and subcellular distribution of the TIGAR were assessed by immunoblotting (Input panels). Immunoprecipitations were performed using Anti-Phospho-Serine or Anti-Phospho-Tyrosine (as a negative control) antibodies and Protein-G agarose beads and the phosphorylated TIGAR protein was resolved by 12.5% Tris-Glycine SDS-PAGE and detected by immunoblotting with densitometric quantitation. The relative Mitochondrial/Cytoplasmic Phospho-Ser Indices were calculated as described in the Materials and methods. Figure 4C demonstrates the hypoxia-independent mitochondrial targeting of TIGAR in the HTLV-1+ ATLL SLB1 T-cell-line was visualized by labeling the cells with MitoTracker Orange (red signal) and then performing immunofluorescence-confocal microscopy using a rabbit polyclonal Anti-TIGAR (M-209) primary antibody (Santa Cruz Biotechnology) and Alexa-Fluor 488-conjugated donkey Anti-Rabbit IgG fluorescent secondary antibody (Jackson Immunoresearch Laboratories; green signal). DAPI nuclear-staining (blue signal) is provided for reference. Scale bar, 20 μm. Figure 4D shows the effects of the chemical kinase inhibitors: Wortmannin (20 nM), staurosporine (12.5 nM), or SB203580 (50 nM) upon the mitochondrial localization of TIGAR in the HTLV-1+ ATLL T-cell-lines, SLB1 (left graph) and MJG11 (right graph), were determined by labeling the treated cells with MitoTracker Orange and then performing immunofluorescence-confocal microscopy using an Anti-TIGAR primary antibody. The colocalization between the MitoTracker Orange and TIGAR-specific fluorescent signals was measured across a standard 5 μm^2 area using the ZEN OS Colocalization tool and Pearson correlation coefficient (Carl Zeiss Microscopy). Twenty individual cells were analyzed for each data point (n-value=20). The data is mean ± SD. N-value=3. The asterisks denote statistical significance as determined using unpaired two-tailed Student's t-tests (**P<0.0021). All the data in Figures 4A-4D is representative of at least three independent experiments (Figure 4).

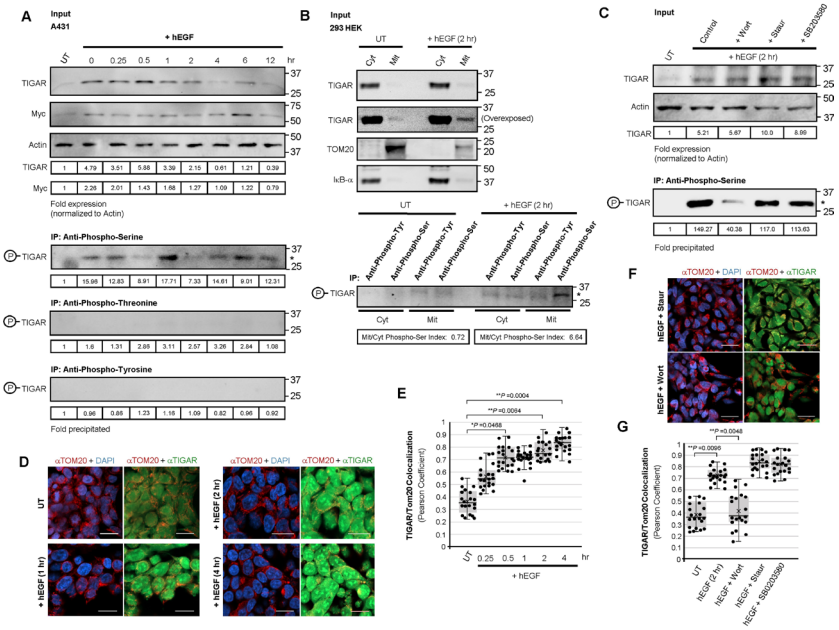

Figure 2: Epidermal growth factor-receptor mitogenic signaling activates TIGAR and induces its serine-phosphorylation and mitochondrial targeting associated with Myc-dependent cellular proliferation.

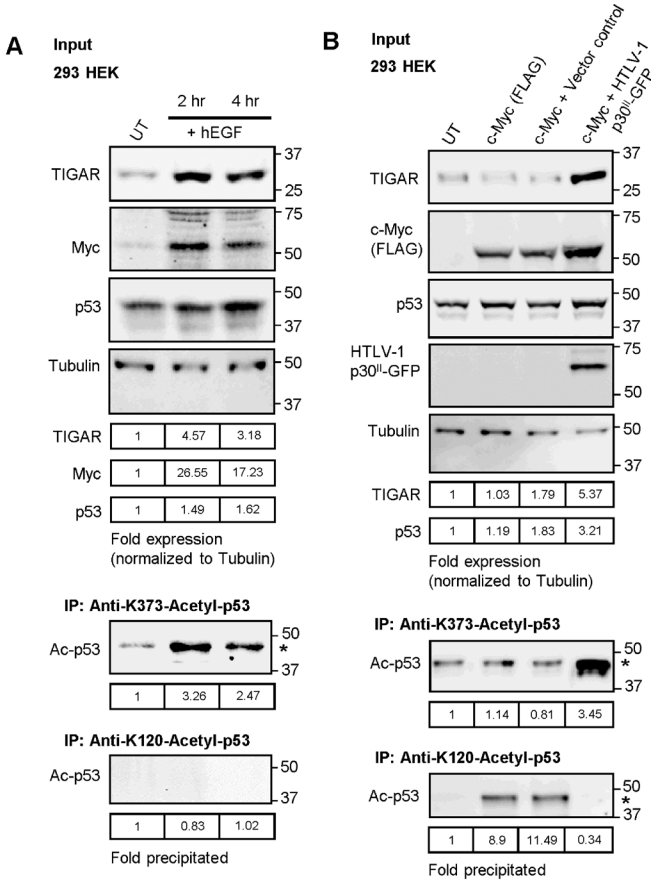

Figure 3: Both HTLV-1 p30II and tyrosine kinase growth factor-receptor-signaling inhibit lysine K120-acetylation of the *p53* protein and induce K373-acetylation of *p53* that correlates with Myc activation.

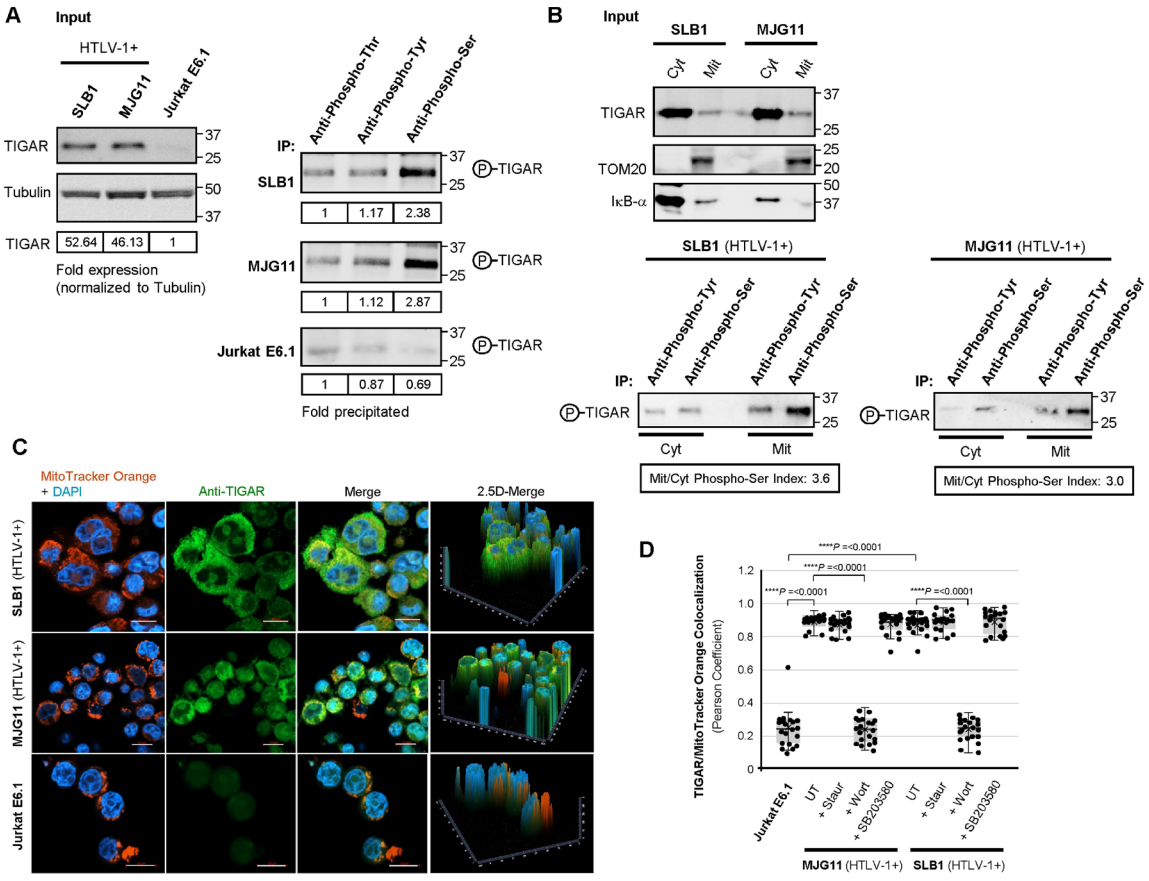

Figure 4: The TIGAR protein is serine-phosphorylated associated with its hypoxia-independent mitochondrial targeting in HTLV-1-transformed ATLL lymphoblasts.

To determine if the TIGAR protects HTLV-1+ ATLL cells against oncogene-induced cytotoxicity, HTLV-1-transformed SLB1 lymphoblasts were transduced with a lentiviral-small interfering RNA-tigar (siRNA-tigar) vector that specifically targets tigar mRNA transcripts and inhibits TIGAR protein expression, compared to an empty lentiviral vector as negative control (Figure 5A) [25]. TIGAR protein levels were analyzed by immunoblotting and quantified by densitometry (Figure 5A). Next, as shown in Figures 5B and 5C, the HTLV-1+ SLB1 ATLL cell-line was transduced with either lentiviral-siRNA-tigar or an empty vector as negative control, and the intracellular accumulation of damaging ROS was detected by staining the cells with a fluorescent chemical ROS probe, CM-H2DCFDA (green signal; Invitrogen), and followed by confocal microscopy analysis. The relative percentages of ROS (CM-H2DCFDA)-positive cells were quantified by counting triplicate visual fields at 200X magnification with comparison to the total numbers of cells in each field (visualized using a Differential Interference Contrast (DIC) filter). These data demonstrate that the lentiviral-siRNA-inhibition of TIGAR resulted in the accumulation of cytotoxic ROS in transduced HTLV-1+ SLB1 lymphoblasts (Figures 5B and 5C).

Lentiviral-siRNA-inhibition of TIGAR prevents HTLV-1-induced tumorigenesis and CNS metastasis in engrafted NOD/scid animals

We next tested whether the lentiviral-siRNA-tigar knockdown of TIGAR could inhibit lymphomagenesis *in vivo* by a tumorigenic HTLV-1+ SLB1-Green Fluorescent Protein (GFP) T-cell-line that is stably transduced with lentiviral-GFP [39]. For these studies, immunodeficient NOD/scid mice (n=3 per sample group) were anesthetized and then injected intraperitoneally with either a Vehicle control (i.e., sterile Ca^{2+}/Mg^{2+}-free PBS, pH 7.4), or 1 x 106 HTLV-1+ SLB-GFP cells that were transduced with a pLenti empty vector or pLenti-siRNA-tigar expression vector. The animals were housed in an IVC rack and monitored closely for signs of tumor development (e.g., abdominal distension, weight loss, or lethargy), distress, or general morbidity (e.g., rough fur, difficulty with ambulation, eating, or drinking). After 10-12 weeks, the animals were humanely sacrificed and necropsies were performed to harvest the primary tumor tissues and any affected secondary organs (spleen, liver, pancreas, and brain). Two-out-of-three of the SLB-GFP/pLenti vector animals developed submandibular lymphoma tumors with corresponding enlargement of the spleen, CNS metastasis, and severe neurological symptoms i.e., a 'rolling' phenotype that resembled cerebellar ataxia; (Figures 5D and 5E) [84]. No tumors or other pathology was observed in the Vehicle control or SLB1-GFP/pLenti-siRNA-tigar experimental animals (Figures 5D and 5E). Intriguingly, we discovered the HTLV-1+ SLB1-GFP/pLenti tumor cells had metastasized to the brain and were primarily present in the cerebellum of the two animals which had lymphomas and exhibited neurological dysfunction. The brain tissues from these mice showed obvious tissue pathologies as compared to the brains of the SLB1-GFP/pLenti-siRNA-tigar animals (Figure 5F). While we recognize the preliminary nature of these findings due to the small number of animals used, these results demonstrate that the inhibition of TIGAR correlates with reduced HTLV-1 tumorigenesis *in vivo*; and the FACS-isolation of brain metastatic SLB1-GFP/pLenti tumor cells for transcriptome analysis could yield valuable insight into the mechanisms that govern CNS homing associated with brain metastasis during ATLL or the CNS targeting of HTLV-1+ T-lymphocytes related to HAM/TSP (Figure 5A).

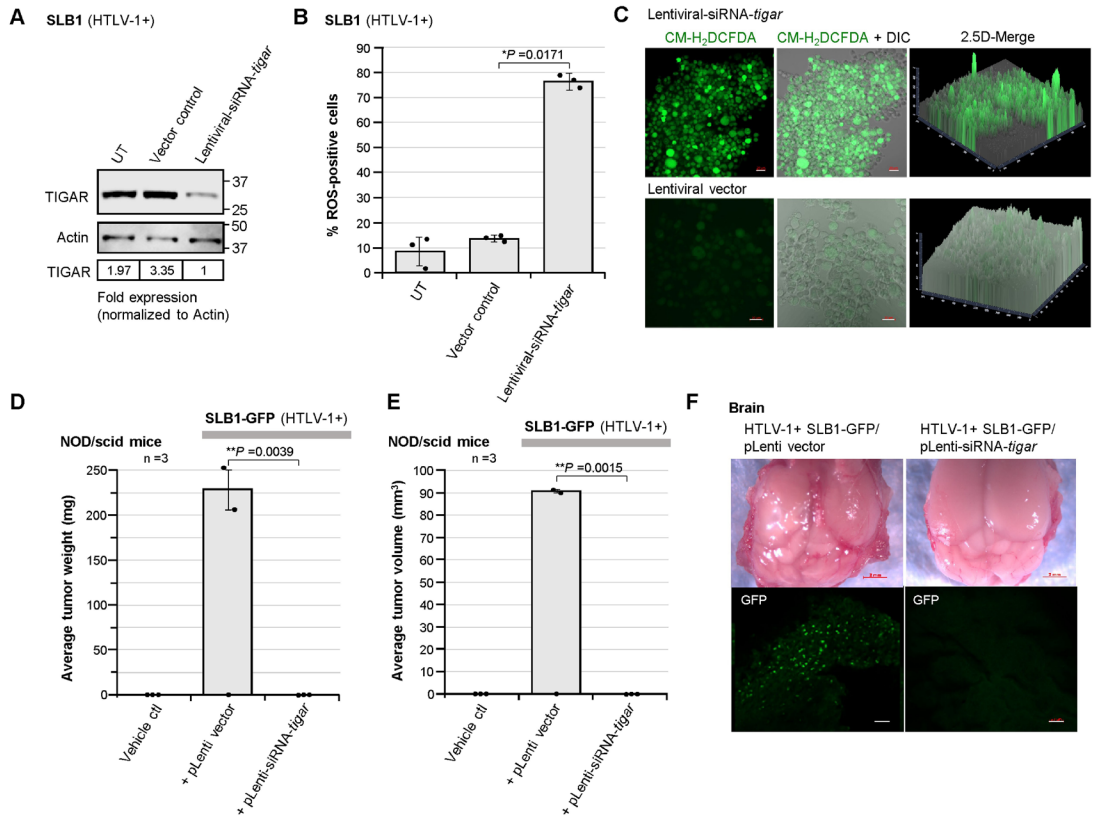

Figure 5: siRNA-knockdown of TIGAR expression leads to the accumulation of damaging ROS in HTLV-1-transformed ATLL cells and inhibits tumorigenesis *in vivo*.

HTLV-1-transformed ATLL SLB1 T-cells were transduced with either a lentiviral siRNA-tigar expression vector or an empty lentiviral (pLenti 6.2/V5-DEST) vector as negative control, and the relative expression of TIGAR was detected by immunoblotting and quantified by densitometry with normalization to Actin. UT, untransduced cells. (Figure 5B and 5C) HTLV-1+ SLB1 T-cells were plated on an 8-chamber tissue-culture slide and then transduced as in A. The intracellular accumulation of ROS was visualized by staining the cells with a chemical ROS-specific fluorescent probe, CM-H2DCFDA (Invitrogen; green signal), and then performing confocal microscopy. Scale bar, 20 μm. A differential interference contrast (DIC) filter was included in merged images to visualize all cells within the field. Graphical 2.5D merged images (CM-H2DCFDA + DIC) are shown at right in C. The relative percentages of ROS (CM-H2DCFDA)-positive HTLV-1+ ATLL SLB1 cells were quantified by confocal microscopy and counting each visual field in-triplicate at 200X magnification. The data is mean ± SD. N-value=3. The asterisks denote statistical significance as determined using unpaired two-tailed Students t-tests (**P<0.0021). Figures 5D and 5E shows Immunodeficient NOD/scid mice were injected intraperitoneally with a Vehicle control or HTLV-1+ SLB1-GFP lymphoblasts that were transduced with a pLenti empty vector or pLenti-siRNA-tigar (n=3 per sample group). After 10-12 weeks, the animals were humanely sacrificed and the primary tumors were weighed and their volumes were calculated by measuring with a digital caliper. Figure F demonstrates Brain pathology and CNS (cerebellar) metastases were observed in two HTLV-1+ SLB1-GFP/pLenti vector animals which had lymphoma tumors and exhibited neurological symptoms, as compared to the SLB1-GFP/pLenti-siRNA-tigar mice (see green cells in lower left panel). Scale bar, 20 μm.

These comparative studies have shown that both the HTLV-1 latency-maintenance factor p30II and tyrosine kinase-receptor signaling modulate the posttranslational acetylation of TP53 and induce the serine-phosphorylation and mitochondrial targeting of TIGAR which protects proliferating cells against metabolic oxidative stress and genotoxicity through potentially analogous mechanisms.

DISCUSSION

In the present study, we have demonstrated that the HTLV-1 latency-maintenance factor p30II augments *p53* lysine K373-acetylation and induces the expression and mitochondrial targeting of TIGAR by inducing its serine-phosphorylation in a manner analogous to tyrosine kinase receptor-signaling. Although p30II represses the expression of HTLV-1 antigens, the p30II protein interacts with the Myc protooncogene and promotes S-phase cell-cycle progression and aberrant proliferation of p30II-expressing T-lymphocytes [2,25,47,58]. Awasthi have demonstrated that the endogenous p30II protein is recruited to Myc-containing TRRAP/NuA4 transactivation complexes on the cyclin D2 gene promoter in HTLV-1-transformed ATLL T-cell-lines (MJG11, HuT-102, ATL-1) [47]. Through biochemical *in vitro* binding studies using purified recombinant HTLV-1 p30II-Glutathione-S-Transferase (GST) fusion proteins (wild-type and deletion mutants) and co-immunoprecipitations in transfected cells, aa residues 99-154 of p30II were found to interact with the acetyltransferase TIP60, also known as Kat5 [2,47]. TIP60 is a transcriptional cofactor for both c-Myc and *p53* [48,50-52,61,85] and several studies have shown that acetylation of the *p53* tumor suppressor on lysine residue K120 by TIP60 differentially regulates the *p53*-dependent expression of pro-apoptotic genes [51-53]. Indeed, we have previously demonstrated that p30II inhibits TIP60-mediated K120-acetylation of the *p53* tumor suppressor and induces *p53*-dependent expression of the TIGAR which mediates the oncogenic cooperation between p30II and other viral (Tax, HBZ) or cellular (c-Myc) oncoproteins by suppressing the accumulation of oncogene-induced ROS [25,37]. Affymetrix U133 microarray analysis using a dominant-negative TIP60 mutant identified 250 genes whose expression was modulated by the HTLV-1 p30II protein, either in a TIP60-dependent or TIP60-independent manner [47].

The p30II protein is essential for the establishment of a persistent infection and the maintenance of a high proviral titer *in vivo*; and rabbits inoculated with irradiated human T-cell-lines expressing an infectious p30II-defective mutant of the HTLV-1 ACH molecular clone exhibited reduced proviral PBMC loads as compared to the wild-type ACH provirus [19,20]. Furthermore, DNA-sequencing revealed that the provirus-positive animals that had been inoculated with the mutant ACH.p30.1 clone exhibited reversion back to the wild-type ACH nucleotide sequence [20]. Also, Willems have shown that deletion of the R3 and G4 open reading frames (which are analogous to the HTLV-1 p30II/p13II and p12I products) in the Bovine Leukemia Virus (BLV) resulted in diminished infectivity and viral transmission *in vivo* in BLV-infected sheep, consistent with an essential role for p30II in retroviral pathogenesis [86]. Valeri have further demonstrated that p30II is required for viral persistence and replication in infected rhesus macaques, and that a p30II-defective mutant HTLV-1 provirus was impaired for its ability to replicate in human dendritic cells which could serve as an *in vivo* reservoir for the virus [21].

Although, the p30II protein contains a functional Transcriptional Activation Domain (TAD), spanning a residues 62-220, which induces CREB-dependent transactivation, the p30II protein has been shown to interact with the transcriptional coactivator/histone acetyltransferase p300 and inhibits the formation of Tax/CREB/p300/Tax-Responsive Element (TRE) quaternary complexes on the viral promoter and blocks Tax-dependent HTLV-1 LTR transactivation which was countered through the exogenous expression of p300 or the p300 Kinase-Inducible Exchange (KIX) domain [2,12-14,87]. Also, the p30II protein interacts with the viral Rex protein and the cellular nuclear export factor CRM-1 in nucleolar foci and negatively regulates Tax-dependent HTLV-1 proviral gene expression and replication by preventing the nuclear export of tax/rex pX mRNA transcripts [15,16,88]. The trans expression of p30II as well as its HTLV-2 synologue, p28II, from cDNAs has been shown to inhibit the functions of the proviral Tax-1/2 and Rex-1/2 proteins and to repress HTLV-1 and HTLV-2 gene expression *in vitro* [16]. However, unlike p30II, the HTLV-2 p28II protein lacks a functional TAD and there is no evidence that p28II directly modulates cellular or viral transcription [89]. Using a p28II-deleted HTLV-2 proviral clone, the p28II protein was shown to be essential for *in vivo* replication and the survival of HTLV-2 provirus-positive cells *in vivo* in infected rabbits [89]. The ability of HTLV-1 p30II (and the HTLV-2 synologue p28II) to suppress the expression of viral antigens and induce proviral latency and inhibit innate pro-inflammatory IFN-γ signaling are likely key to its essential roles in HTLV-1 pathogenesis and persistence *in vivo*.

Baydoun have reported that p30II inhibits homology-directed DNA damage-repair and postulated that p30II could promote the accumulation of genetic mutations and thus increase the risk of oncogenic transformation [90]. Indeed, these findings are

in agreement with our data demonstrating that p30II induces S-phase progression and genomic DNA-endoreduplication [47,58], cooperates with cellular (c-Myc) and other viral (Tax and HBZ) oncoproteins and induces oncogenic transformation/foci formation [37,47,58] as well as the long-term proliferation beyond crisis/immortalization of primary human PBMCs [25], and enhances the *in vitro* survival of cellular clones expressing the infectious HTLV-1 ACH provirus [91]. With the present study, we have addressed the intriguing question of whether the ability of the viral p30II protein to suppress Myc-induced oxidative stress and cytotoxicity through the activation of TIGAR mechanistically resembles the induction of Myc-dependent S-phase entry by tyrosine kinase receptors in normal proliferating cells.

The activation of mitogenic growth factor receptor-signaling induces the expression of protooncogenes, including c-Myc and c-Fos, associated with genomic DNA-replication and cellular proliferation [65,66,92,93]. In particular, tyrosine kinase receptors, such as the EGFR (or Erbb2), enhance Myc-dependent transactivation upon ligand-binding which stimulates the expression of downstream Myc-responsive proliferative genes (e.g., cyclin D2) containing E-box (CACGTG) enhancer elements within their promoters. Leone have shown that the induction of cyclin E-cdk2 proliferative activity and the entry of cells into S-phase are dependent upon cooperation between Ras and Myc [94]. As *p53* is a downstream target of Myc [30-35,61,77], we thus investigated whether tyrosine kinase-receptors which activate Myc might inhibit p53-K120-acetylation and induce TIGAR to promote mitogenic cell proliferation and protect against Myc-associated oxidative stress and cytotoxicity. Indeed, the data in Figures 2A-2G and 3A demonstrate that hEGF-stimulation resulted in increased TIGAR protein expression that correlated with the induction of the Myc protooncogene. Also, growth factor receptor-signaling resulted in the increased phosphorylation of the TIGAR protein on serine residues and correlated with its hypoxia-independent targeting to mitochondrial membranes (Figures 2A-2G). The hEGF-induced phosphorylation and mitochondrial localization of TIGAR were inhibited by treatment with the chemical kinase inhibitor, wortmannin, but not staurosporine or SB203580 (Figures 2C, 2F, and 2G). Interestingly, the data in Figure 3A demonstrate that, although hEGF-receptor-signaling resulted in increased Myc expression, this did not coincide with p53-K120-acetylation, but rather, led to enhanced p53-K373-acetylation which is associated with p300 activity [81,95]. As the recruitment of TIP60 to *p53* requires methylation of the *p53* tumor suppressor on lysine residue K372 by the methyltransferases Set7/9 which facilitates binding by the TIP60 chromodomain [53], it is possible that acetylation by p300 may have prevented the recruitment of Set7/9 and inhibited *p53* K372-metylation. We further observed that the HTLV-1 p30II protein inhibited TIP60-mediated acetylation of *p53* on lysine K120 in response to oncogenic c-Myc expression and resulted in increased *p53* K373-acetylation (Figure 3B). The activation of TIGAR by either EGFR-signaling or the viral p30II protein coincided with the inhibition of *p53* K120-acetylation and induction of p53 K373-acetylation, suggesting that p30II modulates the posttranslational modifications of *p53* and induces TIGAR through a conserved mechanism which resembles tyrosine kinase growth factor-receptor-signaling. The TIGAR protein was phosphorylated on serine residues in HTLV-1-transformed ATLL T-cell-lines (i.e., MJG11, HuT1-2, and SLB1), as compared to Jurkat lymphocytes, associated with its hypoxia-independent localization to mitochondrial membranes (Figures 4A and 4B). Similar to the results obtained for HTLV-1 p30II-GFP in transfected cells, the phosphorylation and mitochondrial targeting of TIGAR in HTLV-1+ ATLL cells was blocked by the chemical inhibitor of phosphoinositide kinases, wortmannin, but not by staurosporine or SB203580 (Figure 4D). Importantly, siRNA-knockdown of TIGAR expression resulted in the intracellular accumulation of damaging ROS in the HTLV-1+ ATLL SLB1 cell-line (Figures 5A-5C) and inhibited lymphomagenesis *in vivo* in NOD/scid mice that were IP engrafted with lentiviral siRNA-tigar-transduced HTLV-1+ SLB1-GFP cells (Figures 5D and 5E). Whereas CNS (cerebellar) metastasis and aberrant brain lesions were observed in some HTLV-1+ SLB1-GFP/pLenti vector animals which exhibited T-cell lymphomas and neurological ataxia-like symptoms, the lentiviral siRNA-knockdown of TIGAR markedly inhibited HTLV-1 tumorigenesis and CNS metastasis in the experimental animals (Figures 5D-5F).

CONCLUSION

These findings allude to a key pro-survival role for the activation of TIGAR's mitochondrial antioxidant functions by the viral p30II protein in HTLV-1-associated lymphopathogenesis and the development and progression of ATLL. Although the specific site(s) of serine-phosphorylation within the TIGAR protein associated with its translocation to mitochondrial membranes remains to be biochemically identified, there are putative MAPK D-motif target sequences at aa residues 203-209 and 214-224 and an S/P site at positions 157-163 which could be phosphorylated by the HTLV-1 p30II oncoprotein and/or tyrosine kinase growth factor receptor-signaling. Our present studies have shown that Serphosphorylation is required for the trafficking of TIGAR to mitochondria and the suppression of damaging oncogene-induced ROS. There are several possible mechanisms whereby phosphosignaling could regulate the subcellular translocation of TIGAR: 1) Ser-phosphorylation could promote molecular interactions between TIGAR and HK2 or another cellular factor on the outer membranes of mitochondria, or alternatively; 2) The phosphorylated TIGAR protein might be recognized by a molecular chaperone that contains a Mitochondrial Targeting Sequence (Mts). Our results further suggest that targeting the TIGAR protein may be a plausible antiviral/antiretroviral strategy to treat HTLV-1-induced hematological cancers. Moreover, as the upregulation of TIGAR has been linked with therapy-resistance and aggressive disease phenotypes for many types of cancers, including malignant gliomas, esophageal, nasopharyngeal, gastric, renal cell, and HPV+ cervical carcinomas, in addition to multiple myeloma, lymphoblastic leukemia, acute myeloid leukemia, ATLL, and chronic lymphocytic leukemia, the ability to therapeutically target TIGAR or the kinases that regulate its antioxidant functions could have broader implications for the treatment of viral and non-viral cancers.

CONFLICTS OF INTEREST

The authors declare there are no conflicts of interest.

DATA AVAILABILITY

All data are contained within the article.

ACKNOWLEDGEMENT

The authors thank S.B. McMahon for the CβF-c-Myc (FLAG-tagged) expression construct and P. Green for kindly providing the HTLV-1+ adult T-cell lymphoma SLB1 cell-line. We also thank other members of the Harrod lab: J. Wilbourne and C. Harrod, for technical assistance.

CREDIT AUTHORSHIP CONTRIBUTION STATEMENT

Tetiana Bowley: Conceptualization, Methodology, Validation, Formal analysis, Investigation, Data curation, Visualization, Writing-review and editing. Aditi Malu: Conceptualization, Methodology, Validation, Formal analysis, Investigation, Data curation, Writing-review and editing. Natalie Adams: Formal analysis, Investigation. Julia Savage: Formal analysis, Investigation. Melika Saberi: Formal analysis, Investigation. Mya VanderHagen: Formal analysis, Investigation. Reena Alame: Formal analysis, Investigation. Makenna Keating: Formal analysis, Investigation. Courtney Yates: Formal analysis, Resources. Robert Harrod: Conceptualization, Methodology, Validation, Formal analysis, Investigation, Data curation, Visualization, writing–original draft, Writing-review and editing, Supervision, Project administration, Funding acquisition.

FUNDING SOURCE

This work was supported by a National Cancer Institute/National Institutes of Health grant 1R15CA267892-01A1 to RH. TB was also supported by an American Society for Microbiology-Graduate Student Fellowship.

REFERENCES

1. Willems L, Hasegawa H, Accolla R, Bangham C, Bazarbachi A, Bertazzoni U, et al. Reducing the global burden of HTLV-1 infection: An agenda for research and action. Antiviral Res. 2017;137:41-48.
2. Harrod R. Silencers of HTLV-1 and HTLV-2: The pX-encoded latency-maintenance factors. Retrovirology. 2019;16(1):25.
3. Mahieux R, Gessain A. Adult T-cell leukemia/lymphoma and HTLV-1. Curr Hematol Malig Rep. 2007;2:257-264.
4. Pais-Correia AM, Sachse M, Guadagnini S, Robbiati V, Lasserre R, Gessain A, et al. Biofilm-like extracellular viral assemblies mediate HTLV-1 cell-to-cell transmission at virological synapses. Nat Med. 2010;16:83-89.
5. Igakura T, Stinchcombe JC, Goon PKC, Taylor GP, Weber JN, Griffiths GM, et al. Spread of HTLV-I between lymphocytes by virus-induced polarization of the cytoskeleton. Science. 2003;299:1713-1716.
6. Van Prooyen N, Gold H, Andresen V, Schwartz O, Jones K, Ruscetti F, et al. Human T-cell leukemia virus type 1 p8 protein increases cellular conduits and virus transmission. Proc Natl Acad Sci. 2010;107:20738-20743.
7. Legrand N, McGregor S, Bull R, Bajis S, Valencia BK, Ronnachit A, et al. Clinical and public health implications of human T-lymphotropic virus type 1 infection. Clin Microbiol Rev. 2022;35:e0007821.
8. Johnson JM, Harrod R, Franchini G. Molecular biology and pathogenesis of the Human T-cell Leukaemia/Lymphotropic Virus Type-1 (HTLV-1). Int J Exp Pathol. 2001;82:135-147.
9. Lemasson I, Lewis MR, Polakowski N, Hivin P, Cavanaugh MH, Thebault S, et al. Human T-cell leukemia virus type 1 (HTLV-1) bZIP protein interacts with the cellular transcription factor CREB to inhibit HTLV-1 transcription. J Virol. 2007;81:1543-1553.
10. Clerc I, Polakowski N, Andre-Arpin C, Cook P, Barbeau B, Mesnard JM, et al. An interaction between the human T cell leukemia virus type 1 basic leucine zipper factor (HBZ) and the KIX domain of p300/CBP contributes to the down-regulation of tax-dependent viral transcription by HBZ. J Biol Chem. 2008;283:23903-23913.
11. Andresen V, Pise-Masison CA, Sinha-Datta U, Bellon M, Valeri V, Parks RW, et al. Suppression of HTLV-1 replication by Tax-mediated rerouting of the p13 viral protein to nuclear speckles. Blood. 2011;118:1549-1559.
12. Zhang W, Nisbet JW, Bartoe JT, Ding W, Lairmore MD. Human T-lymphotropic virus type 1 p30(II) functions as a transcription factor and differentially modulates CREB-responsive promoters. J Virol. 2000;74:11270-11277.
13. Zhang W, Nisbet JW, Albrecht B, Ding W, Kashanchi F, Bartoe JT, et al. Human T- lymphotropic virus type 1 p30(II) regulates gene transcription by binding CREB binding protein/p300. J Virol. 2001;75:9885-9895.
14. Michael B, Nair AM, Datta A, Hiraragi H, Ratner L, Lairmore MD. Histone Acetyltransferase (HAT) activity of p300 modulates human T lymphotropic virus type 1 p30II-mediated repression of LTR transcriptional activity. Virology 2006;354:225-239.
15. Nicot C, Dundr M, Johnson JM, Fullen JR, Alonzo N, Fukumoto R, et al. HTLV-1-encoded p30II is a post-transcriptional negative regulator of viral replication. Nat Med. 2004;10:197-201.
16. Younis I, Khair L, Dundr M, Lairmore MD, Franchini G, Green PL. Repression of human T- cell leukemia virus type 1 and 2 replication by a viral mRNA-encoded posttranscriptional regulator. J Virol. 2004;78:11077-11083.
17. Koralnik IJ, Gessain A, Klotman ME, Lo Monico A, Berneman ZN, Franchini G. Protein isoforms encoded by the pX region of human T-cell leukemia/lymphotropic virus type I. Proc Natl Acad Sci. 1992;89: 8813-8817.
18. Cereseto A, Berneman Z, Koralnik I, Vaughn J, Franchini G, Klotman ME. Differential expression of alternatively spliced pX mRNAs in HTLV-I-infected cell lines. Leukemia 1997;11:866-870.
19. Bartoe JT, Albrecht B, Collins ND, Ratner L, Green PL, Lairmore MD. Functional role of pX open reading frame II of human T-lymphotropic virus type 1 in maintenance of viral loads *in vivo*. J Virol. 2000;74:1094-1100.
20. Silverman LR, Phipps AJ, Montgomery A, Ratner L, Lairmore MD. Human T-cell lymphotropic virus type 1 open reading frame II-encoded p30II is required for *in vivo* replication: Evidence of *in vivo* reversion. J Virol. 2004;78:3837-3845.
21. Valeri VW, Hryniewicz A, Andresen V, Jones K, Fenizia C, Bialuk I, et al. Requirement of the human T-cell leukemia virus p12 and p30 products for infectivity of human dendritic cells and macaques but not rabbits. Blood. 2010;116:3809-3817.
22. Pique C, Ureta-Vidal A, Gessain A, Chancerel B, Gout O, Tamouza R, et al. Evidence for the chronic *in vivo* production of human T cell leukemia virus type I Rof and Tof proteins from cytotoxic T lymphocytes directed against viral peptides. J Exp Med. 2000;191:567-572.
23. Pise-Masison CA, Mahieux R, Jiang H, Ashcroft M, Radonovich M, Duvall J, et al. Inactivation of p53 by human T-cell lymphotropic virus type 1 Tax requires activation of the NF-kappaB pathway and is dependent on *p53* phosphorylation. Mol Cell Biol. 2000;20:3377-3386.
24. Zane L, Yasunaga J, Mitagami Y, Yedavalli V, Tang SW, Chen CY, et al. Wip1 and *p53* contribute to HTLV-1 Tax-induced tumorigenesis. Retrovirology. 2012;9:114.
25. Romeo M, Hutchison T, Malu A, White A, Kim J, Gardner R, et al. The human T-cell leukemia virus type-1 p30II protein activates *p53* and induces the TIGAR and suppresses oncogene-induced oxidative stress during viral carcinogenesis. Virology. 2018;518:103-115.
26. Bensaad K, Tsuruta A, Selak MA, Vidal MN, Nakano K, Bartrons R, et al. TIGAR, a *p53*-inducible regulator of glycolysis and apoptosis. Cell. 2006;126:107-120.
27. Bensaad K, Cheung EC, Vousden KH. Modulation of intracellular

ROS levels by TIGAR controls autophagy. EMBO J. 2009;28:3015-3026.

28. Cheung EC, Athineos D, Lee P, Ridgway RA, Lambie W, Nixon C, et al. TIGAR is required for efficient intestinal regeneration and tumorigenesis. Dev Cell. 2013;25:463-477.

29. Cheung EC, Lee P, Ceteci F, Nixon C, Blyth K, Sansom OJ, et al. Opposing effects of TIGAR- and RAC1-derived ROS on Wnt-driven proliferation in the mouse intestine. Genes Dev. 2016;30:52-63.

30. Vafa O, Wade M, Kern S, Beeche M, Pandita TK, Hampton GM, et al. c-Myc can induce DNA damage, increase reactive oxygen species, and mitigate *p53* function: A mechanism for oncogene-induced genetic instability. Mol Cell. 2002;9:1031-1044.

31. Reisman D, Elkind NB, Roy B, Beamon J, Rotter V. c-Myc transactivates the *p53* promoter through a required downstream CACGTG motif. Cell Growth Differ. 1993;4:57-65.

32. Chen L, Iraci N, Gherardi S, Gamble LD, Wood KM, Perini G, et al. *P53* is a direct transcriptional target of MYCN in neuroblastoma. Cancer Res. 2010;70:1377-1388.

33. Roy B, Beamon J, Balint E, Reisman D. Transactivation of the human *p53* tumor suppressor gene by c-Myc/Max contributes to elevated mutant *p53* expression in some tumors. Mol Cell Biol. 1994;14:7805-7815.

34. Hermeking H, Eick D. Mediation of c-Myc-induced apoptosis by *p53*. Science. 1994;265:2091-2093.

35. Zindy F, Eischen CM, Randle DH, Kamijo T, Cleveland JL, Sherr CJ, et al. Myc signaling via the ARF tumor suppressor regulates *p53*-dependent apoptosis and immortalization. Genes Dev. 1998;12:2424-2433.

36. Wagner AJ, Kokontis JM, Hay N. Myc-mediated apoptosis requires wild-type *p53* in a manner independent of cell scycle arrest and the ability of *p53* to induce p21waf1/cip1. Genes Dev. 1994;8:2817-2830.

37. Hutchison T, Malu A, Yapindi L, Bergeson R, Peck K, Romeo M, et al. The T*P53*-Induced glycolysis and apoptosis regulator mediates cooperation between HTLV-1 p30II and the retroviral oncoproteins Tax and HBZ and is highly expressed in an *in vivo* xenograft model of HTLV- 1-induced lymphoma. Virology. 2018;520:39-58.

38. Cheung EC, Ludwig RL, Vousden KH. Mitochondrial localization of TIGAR under hypoxia stimulates HK2 and lowers ROS and cell death. Proc Natl Acad Sci. 2012;109:20491-20496.

39. Hutchison T, Yapindi L, Malu A, Newman RA, Sastry KJ, Harrod R. The botanical glycoside oleandrin inhibits human T-cell leukemia virus type-1 infectivity and Env-dependent virological synapse formation. J Antivir Antiretrovir. 2019;11(3):184.

40. McMahon SB, Van Buskirk HA, Dugan KA, Copeland TD, Cole MD. The novel ATM-related protein TRRAP is an essential cofactor for the c-Myc and E2F oncoproteins. Cell. 1998;94:363-374.

41. Yapindi L, Bowley T, Kurtaneck N, Bergeson RL, James K, Wilbourne J, et al. Activation of *p53*-regulated pro-survival signals and hypoxia-independent mitochondrial targeting of TIGAR by human papillomavirus E6 oncoproteins. Virology. 2023;585:1-20.

42. Lee P, Hock AK, Vousden KH, Cheung EC. *P53*- and p73-independent activation of TIGAR expression *in vivo*. Cell Death Dis. 2015;6:e1842.

43. Simon-Molas H, Sánchez-de-Diego C, Navarro-Sabaté A, Castaño E, Ventura F, Bartrons R, et al. The expression of T*P53*-Induced Glycolysis and Apoptosis Regulator (TIGAR) can be controlled by the antioxidant orchestrator NRF2 in human carcinoma cells. Int J Mol Sci. 2022;23:1905.

44. Eriksson SE, Ceder S, Bykov VJN, Wiman KG. *P53* as a hub in cellular redox regulation and therapeutic target in cancer. J Mol Cell Biol. 2019;11:330-341.

45. Sun M, Li M, Huang Q, Han F, Gu JH, Xie J, et al. Ischemia/reperfusion- induced upregulation of TIGAR in brain is mediated by SP1 and modulated by ROS and hormones involved in glucose metabolism. Neurochem Int. 2015;80:99-109.

46. Zou S, Wang X, Deng L, Wang L, Wang Y, Huang B, et al. CREB, another culprit for TIGAR promoter activity and expression. Biochem Biophys Res Commun. 2013;439:481-486.

47. Awasthi S, Sharma A, Wong K, Zhang J, Matlock EF, Rogers L, et al. A human T-cell lymphotropic virus type 1 enhancer of Myc transforming potential stabilizes Myc-TIP60 transcriptional interactions. Mol Cell Biol. 2005;25:6178-6198.

48. Frank SR, Parisi T, Taubert S, Fernandez P, Fuchs M, Chan HM, et al. MYC recruits the TIP60 histone acetyltransferase complex to chromatin. EMBO Rep. 2003;4:575-580.

49. Zhao LJ, Loewenstein PM, Green M. Identification of a panel of MYC and TIP60 co-regulated genes functioning primarily in cell cycle and DNA replication. Genes Cancer. 2018;9:101-113.

50. Patel JH, Du Y, Ard PG, Phillips C, Carella B, Chen CJ, et al. The c-Myc oncoprotein is a substrate of the acetyltransferases hGCN5/PCAF and TIP60. Mol Cell Biol. 2004;24:10826-10834.

51. Tang Y, Luo J, Zhang W, Gu W. Tip60-dependent acetylation of *p53* modulates the decision between cell-cycle arrest and apoptosis. Mol Cell. 2006;24:827-839.

52. Sykes SM, Mellert HS, Holbert MA, Li K, Marmorstein R, Lane WS, et al. Acetylation of the *p53* DNA-binding domain regulates apoptosis induction. Mol Cell. 2006;24:841-851.

53. Kurash JK, Lei H, Shen Q, Marston WL, Granda BW, Fan H, et al. Methylation of *p53* by Set7/9 mediates *p53* acetylation and activity *in vivo*. Mol Cell. 2008;29:392-400.

54. Dar A, Shibata E, Dutta A. Deubiquitination of Tip60 by USP7 determines the activity of the *p53*-dependent apoptotic pathway. Mol Cell Biol. 2013;33:3309-3320.

55. Legube G, Linares LK, Tyteca S, Caron C, Scheffner M, Chevillard-Briet M, et al. Role of the histone acetyl transferase Tip60 in the *p53* pathway. J Biol Chem. 2004;279:44825-44833.

56. Wang P, Bao H, Zhang XP, Liu F, Wang W. Regulation of Tip60-dependent *p53* acetylation in cell fate decision. FEBS Lett. 2019;593:13-22.

57. Xu Y, Liao R, Li N, Xiang R, Sun P. Phosphorylation of Tip60 by p38 regulates *p53*- mediated PUMA induction and apoptosis in response to DNA damage. Oncotarget 2014;5:12555-12572.

58. Romeo MM, Ko B, Kim J, Brady R, Heatley HC, He J, et al. Acetylation of the c-MYC oncoprotein is required for cooperation with the HTLV-1 p30(II) accessory protein and the induction of oncogenic cellular transformation by p30(II)/c-MYC. Virology. 2015;476:271-288.

59. Zhou JH, Zhang TT, Song DD, Xia YF, Qin ZH, Sheng R. TIGAR contributes to ischemic tolerance induced by cerebral preconditioning through scavenging of reactive oxygen species and inhibition of apoptosis. Sci Rep. 2016;6:27096.

60. Li M, Sun M, Cao L, Gu JH, Ge J, Chen J, et al. A TIGAR-regulated metabolic pathway is critical for protection of brain ischemia. J Neurosci. 2014;34:7458-7471.

61. Gorrini C, Squatrito M, Luise C, Syed N, Perna D, Wark L, et al. Tip60 is a haplo-insufficient tumour suppressor required for an oncogene-induced DNA damage response. Nature. 2007;448:1063-1067.

62. Ko A, Han SY, Choi CH, Cho H, Lee MS, Kim SY, et al. Oncogene-induced senescence mediated by c-Myc requires USP10 dependent deubiquitination and stabilization of p14ARF. Cell Death Differ.

2018;25:1050-1062.

63. Campaner S, Doni M, Hydbring P, Verrecchia A, Bianchi L, Sardella D, et al. Cdk2 suppresses cellular senescence induced by the c-myc oncogene. Nat Cell Biol. 2010;12:54-59.

64. Lu D, Wilson C, Littlewood TD. Methods for determining Myc-induced apoptosis. Methods Mol Biol. 2021;2318:209-229.

65. Bravo R, Burckhardt J, Curran T, Müller R. Stimulation and inhibition of growth by EGF in different A431 cell clones is accompanied by the rapid induction of c-fos and c-myc proto- oncogenes. EMBO J. 1985;4:1193-1197.

66. Reiss M, Dibble CL, Narayanan R. Transcriptional activation of the c-myc proto-oncogene in murine keratinocytes enhances the response to epidermal growth factor. J Invest Dermatol. 1989;93:136-141.

67. Zhu L, Chen Z, Zang H, Fan S, Gu J, Zhang G, et al. Targeting c-Myc to overcome acquired resistance of EGFR mutant NSCLC cells to the third-generation EGFR tyrosine kinase inhibitor, Osimertinib. Cancer Res. 2021;81:4822-4834.

68. Yin Y, Sun M, Zhan X, Wu C, Geng P, Sun X, et al. EGFR signal ing confers resistance to BET inhibition in hepatocellular carcinoma through stabilizing oncogenic MYC. J Exp Clin Cancer Res. 2019;38:83.

69. Bouchard C, Thieke K, Maier A, Saffrich R, Hanley-Hyde J, Ansorge W, et al. Direct induction of cyclin D2 by Myc contributes to cell cycle progression and sequestration of p27. EMBO J. 1999;18:5321-5333.

70. Bouchard C, Dittrich O, Kiermaier A, Dohmann K, Menkel A, Eilers M, et al. Regulation of cyclin D2 gene expression by the Myc/Max/Mad network: Myc-dependent TRRAP recruitment and histone acetylation at the cyclin D2 promoter. Genes Dev. 2001;15:2042-2047.

71. Perez-Roger I, Kim SH, Griffiths B, Sewing A, Land H. Cyclins D1 and D2 mediate myc- induced proliferation via sequestration of p27(Kip1) and p21(Cip1). EMBO J. 1999;18:5310-5320.

72. Lui VWY, Wong EYL, Ho K, Ng PKS, Lau CPY, Tsui SKW, et al. Inhibition of c-Met downregulates TIGAR expression and reduces NADPH production leading to cell death. Oncogene 2011;30:1127-1134.

73. Shen M, Zhao X, Zhao L, Shi L, An S, Huang G, et al. Met is involved in TIGAR-regulated metastasis of non-small-cell lung cancer. Mol Cancer 2018;17:88.

74. Kirch HC, Flaswinkel S, Rumpf H, Brockmann D, Es che H. Expression of human *p53* requires synergistic activation of transcription from the *p53* promoter by AP-1, NF-kappaB and Myc/Max. Oncogene. 1999;18:2728-2738.

75. Amente S, Gargano B, Varrone F, Ruggiero L, Dominguez-Sola D, Lania L, et al. p14ARF directly interacts with Myc through the Myc BoxII domain. Cancer Biol Ther. 2006;5:287-291.

76. Eischen CM, Weber JD, Roussel MF, Sherr CJ, Cleveland JL. Disruption of the ARF-Mdm2- *p53* tumor suppressor pathway in Myc-induced lymphomagenesis. Genes Dev. 1999;13:2658-2669.

77. Chen D, Kon N, Zhong J, Zhang P, Yu L, Gu W. Differential effects on ARF stability by normal *versus* oncogenic levels of c-Myc expression. Mol Cell. 2013;51:46-56.

78. Liu N, Wang J, Wang J, Wang R, Liu Z, Yu Y, et al. ING5 is a Tip60 cofactor that acetylates *p53* in response to DNA damage. Cancer Res. 2013;73:3749-3760.

79. Fan QD, Wu G, Liu ZR. Dynamics of posttranslational modifications of *p53*. Comput Math Methods Med. 2014;2014:245610.

80. Squatrito M, Gorrini C, Amati B. Tip60 in DNA damage response and growth control: Many tricks in one HAT. Trends Cell Biol. 2006;16:433-442.

81. Zhao Y, Lu S, Wu L, Chai G, Wang H, Chen Y, et al. Acetylation of *p53* at lysine 373/382 by the histone deacetylase inhibitor depsipeptide induces expression of p21 (Waf1/Cip1). Mol Cell Biol. 2006;26: 2782-2790.

82. Imbriano C, Gurtner A, Cocchiarella F, Di Agostino S, Basile V, Gostissa M, et al. Direct *p53* transcriptional repression: *In vivo* analysis of CCAAT-containing G2/M promoters. Mol Cell Biol. 2005;25:3737-3751.

83. Xiao G, Chicas A, Olivier M, Taya Y, Tyagi S, Kramer FR, et al. A DNA damage signal is required for *p53* to activate gadd45. Cancer Res. 2000;60:1711-1719.

84. Muramoto O, Kanazawa I, Ando K. Neurotransmitter abnormality in Rolling mouse Nagoya, an ataxic mutant mouse. Brain Res. 1981;215:295-304.

85. Faiola F, Liu X, Lo S, Pan S, Zhang K, Lymar E, et al. Dual regulation of c- Myc by p300 via acetylation-dependent control of Myc protein turnover and coactivation of Myc-induced transcription. Mol Cell Biol. 2005;25:10220-10234.

86. Willems L, Kerkhofs P, Dequiedt F, Portetelle D, Mammerickx M, Burny A, et al. Attenuation of bovine leukemia virus by deletion of R3 and G4 open reading frames. Proc Natl Acad Sci, USA. 1994;91:11532-11536.

87. Lairmore MD, Albrecht B, D'Souza C, Nisbet JW, Ding W, Bartoe JT, et al. *In vitro* and *in vivo* functional analysis of human T cell lymphotropic virus type 1 pX open reading frames I and II. AIDS Res Hum Retroviruses. 2000;16:1757-1764.

88. Baydoun H, Duc-Dodon M, Lebrun S, Gazzolo L, Bex F. Regulation of the human T-cell leukemia virus gene expression depends on the localization of regulatory proteins Tax, Rex and p30II in specific nuclear subdomains. Gene. 2007;386:191-201.

89. Yamamoto B, Li M, Kesic M, Younis I, Lairmore MD, Green PL. Human T-cell leukemia virus type 2 post-transcriptional control protein p28 is required for viral infectivity and persistence *in vivo*. Retrovirology. 2008;5:38.

90. Baydoun HH, Pancewicz J, Nicot C. Human T-lymphotropic type 1 virus p30 inhibits homologous recombination and favors unfaithful DNA repair. Blood. 2011;117:5897-5906.

91. Malu A, Hutchison T, Yapindi L, Smith K, Nelson K, Bergeson R, et al. The human T-cell leukemia virus type-1 tax oncoprotein dissociates NF-ΔB p65RelA-Stathmin complexes and causes catastrophic mitotic spindle damage and genomic instability. Virology. 2019;535:83-101.

92. Gulli LF, Palmer KC, Chen YQ, Reddy KB. Epidermal growth factor-induced apoptosis in A431 cells can be reversed by reducing the tyrosine kinase activity. Cell Growth Differ. 1996;7:173-178.

93. Hauguel-DeMouzon S, Csermely P, Zoppini G, Kahn CR. Quantitative dissociation between EGF effects on c-myc and c-fos gene expression, DNA synthesis, and epidermal growth factor receptor tyrosine kinase activity. J Cell Physiol. 1992;150:180-187.

94. Leone G, DeGregori J, Sears R, Jakoi L, Nevins JR. Myc and Ras collaborate in inducing accumulation of active cyclin E/Cdk2 and E2F. Nature. 1997;387:422-426.

95. Knowell AE, Patel D, Morton DJ, Sharma P, Glymph S, Chaudhary J. Id4 dependent acetylation restores mutant-*p53* transcriptional activity. Mol Cancer. 2013;12:161.